Cell Biol Toxicol (2025) 41:88
https://doi.org/10.1007/s10565-025-10040-8

RESEARCH

A novel tsRNA signature -tRF-58:76-Tyr-GTA-2-M3 as potential biomarker and therapeutic target for duodenal atresia

Xinyue Meng · Xiaowei Wei · Hui Gu · Wei Ma · Dan Liu · Shanshan Jia · Songying Cao · Dongxue Ding · Yiwen He · Wanqi Huang · Jia Xue · Wenting Luo · Wei Sun · Zhengwei Yuan

Received: 19 January 2025 / Accepted: 9 May 2025

Abstract Duodenal atresia (DA) is a common neonatal digestive tract obstruction, with unclear prenatal diagnostic specificity and optimal intervention timing. tRNA-derived small RNAs (tsRNAs), stable and enriched in blood, are promising biomarkers for disease diagnosis. Therefore, identifying tsRNA biomarkers, elucidating DA pathogenesis, and exploring potential intrauterine interventions is urgently needed. This study conducts tsRNA profiling via sequencing on plasma samples from pregnant women carrying fetuses with DA and matched healthy controls. Validation was performed in 147 pregnant women, including cohorts with fetal gastrointestinal atresia, normal pregnancies, and post-delivery cases. Functional analyses in cellular models and Adriamycin rat models with DA explored the role of key tsRNAs in DA pathogenesis and intrauterine therapy. It is found that tsRNAs, including tRF-61:78-chrM. Leu-TAA, tRF-60:77-Ile-AAT-1-M4, tRF-57:76-Arg-ACG-1-M2, and tRF-58:76-Tyr-GTA-2-M3, were significantly downregulated in DA cases. tRF-58:76-Tyr-GTA-2-M3 is further implicated in DA development, with knockdown inducing excessive apoptosis via upregulation of SUFU and suppression of GLI1, a hedgehog pathway transcription factor. Intraperitoneal microinjection of tRF-58:76-Tyr-GTA-2-M3 agomir in DA rat models reduce apoptosis and mitigates DA formation by modulating SUFU and GLI1 expression. Taken together, this study identifies novel tsRNA biomarkers for DA, with tRF-58:76-Tyr-GTA-2-M3 playing a pivotal role in its pathogenesis. These findings offer insights into DA mechanisms and suggest potential therapeutic targets, advancing strategies for early diagnosis and intervention.

Keywords Duodenal atresia · Plasma biomarker · TRNA-derived small RNAs · Apoptosis · Intrauterine treatment

Wenting Luo, Wei Sun, and Zhengwei Yuan contributed equally to this work.

Supplementary Information The online version contains supplementary material available at https://doi.org/10.1007/s10565-025-10040-8.

X. Meng · W. Sun (✉)
Department of Ultrasound, Shengjing Hospital of China Medical University, No. 36 Sanhao Street, Heping District, Shenyang 110004, Liaoning, China
e-mail: sunwei8677@126.com

X. Meng · X. Wei · H. Gu · W. Ma · D. Liu · S. Jia · S. Cao · D. Ding · Y. He · W. Huang · J. Xue · W. Luo (✉) · W. Sun · Z. Yuan (✉)
Key Laboratory of Health Ministry for Congenital Malformation, Shengjing Hospital of China Medical University, No. 36 Sanhao Street, Heping District, Shenyang 110004, Liaoning, China
e-mail: lvirginia@163.com

Z. Yuan
e-mail: yuanzw@hotmail.com

Published online: 22 May 2025

Introduction

Duodenal atresia (DA) is defined as congenital intestinal occlusion that occurs in the duodenum. It is one of the most prevalent causes of digestive tract obstruction in newborns, with an incidence of approximately 0.9–1.2 per 10,000 live births and an increasing trend in recent years (Best et al. 2012; Bethell et al. 2020; Hemming and Rankin 2007). DA is an acute abdominal condition in neonates that requires immediate gastrointestinal decompression and surgical intervention. In infants with DA who are not promptly diagnosed before delivery, the likelihood of postoperative complications markedly increases. Furthermore, the duration of parenteral feeding and length of hospital stay are markedly prolonged in some cases, resulting in severe electrolyte imbalances (Basu and Burge 2004; Bittencourt et al. 2004; Patterson et al. 2022; Romero et al. 1988). Such complications profoundly impact the daily lives of affected children, with the potential for considerable adverse effects on their physiological and psychological wellbeing. Currently, there is a dearth of efficacious prenatal diagnostic methods and treatment modalities for DA. Although ultrasound examinations can offer valuable insights, the false-positive and false-negative rate remain an inherent problem due to the reliance on the gestational age of examination and indirect marker such as the "double bubble sign" (Haeusler et al. 2002; Hemming and Rankin 2007). Additionally, maternal serum alpha-fetoprotein levels have been reported to be elevated in pregnant women with DA. However, this biomarker lacks specificity since it may occur in various fetal anomalies, pregnancy complications, placental impairments, and maternal factors (Aboughalia et al. 2020).Therefore, it is imperative to identify more specific molecular markers for non-invasive prenatal diagnosis of DA, as well as to investigate the associated mechanisms and early intervention strategies.

The etiology of DA remains elusive. Tandler's classic"solid cord"hypothesis, proposed in 1900, is widely accepted by most pediatric surgeons. However, it has been criticized for failing to account for the morphological variations in DA and for conflicting with findings from developmental biology research (Botham et al. 2012; Merrot et al. 2006). In recent years, research has focused primarily on *Fgf10-Fgfr2b* axis. Disruption of Fgf10/Fgfr2b signaling represents the most well-established genetic association with DA in murine models (Botham et al. 2012; Fairbanks et al. 2004). Nevertheless, the penetrance of DA in mice deficient for either *Fgf10* or its receptor gene is incomplete, occurring in only 35–75% cases (Fairbanks et al. 2004). Additionally, the Hedgehog signaling pathway has been implicated as a potential contributor to the pathogenesis of congenital gastrointestinal malformations. Mutations in key Hedgehog pathway ligands, such as sonic hedgehog *(Shh)* and indian hedgehog *(Ihh)*, as well as alterations in their downstream signaling components, lead to various severe malformations of the murine gastrointestinal tract, such as esophageal atresia, tracheoesophageal fistula, midgut malrotation, annular pancreas, and duodenal or anal atresia. (Ramalho-Santos et al. 2000; van den Brink 2007). The role of apoptosis in the formation of DA remains a topic of ongoing investigation. Some studies indicate that the absence of *Fgfr2b* expression in the embryonic gastrointestinal tract leads to increased apoptosis, which has been associated with gastrointestinal atresia (Botham et al. 2012; Fairbanks et al. 2006). Conversely, other research posits that apoptosis may not be involved in the pathogenesis of DA (Cheng and Tam 2000). To date, the molecular mechanisms underlying human DA has not been fully clarified.

tRNA-derived small RNAs (tsRNAs) have recently emerged as a distinct class of small noncoding RNAs, generated through site-specific cleavage of precursors or mature tRNAs by specialized ribonucleases (Cole et al. 2009; Lee et al. 2009; Weng et al. 2022). Their extensive post-transcriptional modifications impede adapter ligation and reverse transcription, rendering tsRNAs largely invisible to conventional sequencing workflow. Recent advances in pre-sequencing demethylation and ligation-enhancement techniques have enabled the discovery and validation of an ever-expanding repertoire of tsRNAs in recent years (Shi et al. 2021). tsRNA are typically classified into tRF-1 s, tRF-3 s, tRF-5 s, and tRNA halves (tiRNAs) (Tian et al. 2022). They regulate gene expression through diverse mechanisms such as modulating mRNA stability, inhibiting translation, influencing ribosome biogenesis, and acting as epigenetic regulators. tsRNAs have also been implicated in early embryogenesis. For example, inhibition of tRNA-Gln-TTG-derived small RNAs in mature spermatozoa impairs the first cleavage and subsequent development of porcine embryo (Chen et al. 2020). Comparable

observations have also been documented in human zygotes (Chen et al. 2021). In comparison to conventional diagnostic approaches such as ultrasound and maternal serum biomarkers mentioned above, tsRNAs have the potential to significantly enhance diagnostic sensitivity and specificity due to their stability, tissue-specific expression, and presence in various body fluids, making them promising candidates as biomarkers for disease diagnosis (Shi et al. 2021). To date, aside from the pioneering study by Lu et al. (Lu et al. 2023), which demonstrated that specific tsRNAs can serve as prenatal biomarkers for congenital heart disease, there remains a striking paucity of research characterizing tsRNA expression or function in congenital malformations, and no evidence yet implicates tsRNAs in other developmental defects.

In this study, we conducted tRFs&tiRNAs high-throughput sequencing along with real-time quantitative reverse transcription-polymerase chain reaction (qRT-PCR) in the plasma of pregnant women carrying fetuses diagnosed with DA. The aim of this study was to identify potential tsRNA biomarkers, pathogenesis, and therapeutic targets for DA using human specimens and Adriamycin rat model (ARM). Our findings provide valuable insights into the potential of tsRNAs to enhance prenatal diagnosis and facilitate early intervention in DA.

Materials and methods

Subjects

Study population

Pregnant women were recruited from the ongoing Shengjing Birth Cohort (SJBC), initiated in Northeast China in April 2017. The study included 38 pregnant women carrying fetuses with DA, 23 with jejunal-ileal atresia (JIA), 4 with esophageal atresia (EA), and 65 carrying normal fetuses, followed for at least one year to ensure the infants'health postnatally. For biomarker screening, pregnant women with no fetal anomalies were selected as the control group. To minimize confounding and ensure comparability between the groups, all participants were matched based on gestational age, maternal age, and body mass index (BMI). These factors were chosen as matching criteria due to their known influence on maternal–fetal physiology and potential impact on circulating RNA profiles. Furthermore, 17 paired plasma samples were obtained from women carrying normal fetuses at 38–40 weeks gestation and 24 h post-delivery. Detailed demographics for all groups are provided in Supplementary Table S1, and the overall biomarker screening workflow is illustrated in Supplementary Fig. 1. Diagnoses of DA, JIA, and EA were established via prenatal ultrasonography and postnatal imaging, surgery, or autopsy. Women with multiple pregnancies or other pregnancy-related comorbidities were excluded. Maternal blood samples were collected, centrifuged at 3000 x*g* at 4 °C for 15 min. Plasma samples were stored at −80 °C.

Animal models

Sprague–Dawley rats weighting between 250–300 g were acquired from the Animal Centre of the Shengjing Hospital of China Medical University (Shenyang, Liaoning, China) and mated with conspecifics overnight. Pregnancy was confirmed by examining the genitalia of the females in the presence of sperm the following morning, designated embryonic day 0 (E0). The intraperitoneal injection of adriamycin (1.9 mg/kg on E8–E9; Aladdin, Shanghai, China) is a well-established protocol for generating foregut malformations in the rat that closely resemble human EA/DA in both incidence and histopathology (França et al. 2004; Qi et al. 1996). Administration on E8–E9 targets the critical window of rat foregut patterning, yielding a high penetrance (> 60%) of DA with relatively low maternal mortality. This temporal and dose precision allows us to investigate early molecular events underlying atresia formation in vivo. Pregnant rats were randomly assigned to two groups: one received 1% adriamycin dissolved in saline, while the control group received an equivalent volume of saline alone. Embryos were harvested on E17, E19, and E21, and DA was diagnosed based on duodenal discontinuity under a dissecting microscope.

RNA extraction, pre-treatment and tRF&tiRNA sequencing

Total RNA, including tsRNA derived from plasma of pregnant women, was extracted using TRIzol reagent (Takara, Ohtsu, Japan), following the manufacturer's instructions. RNA purity and concentration were

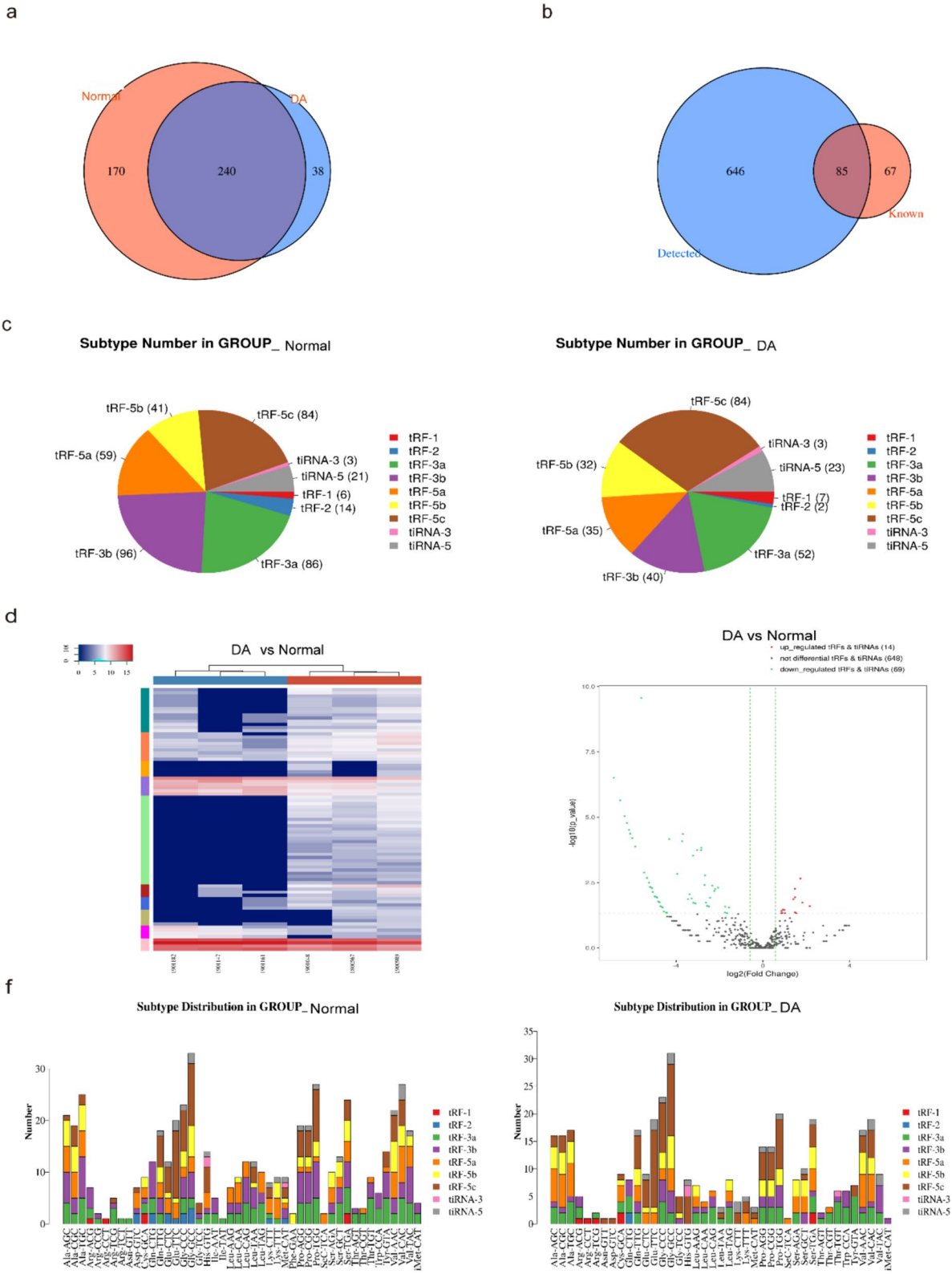
a
Normal
DA
170
240
38
b
646
85
67
Known
Detected
c
Subtype Number in GROUP_ Normal
tRF-5b (41)
tRF-5c (84)
tRF-5a (59)
tiRNA-3 (3)
tiRNA-5 (21)
tRF-1 (6)
tRF-2 (14)
tRF-3b (96)
tRF-3a (86)
Subtype Number in GROUP_ DA
tRF-5c (84)
tiRNA-3 (3)
tRF-5b (32)
tiRNA-5 (23)
tRF-1 (7)
tRF-2 (2)
tRF-5a (35)
tRF-3a (52)
tRF-3b (40)
tRF-1
tRF-2
tRF-3a
tRF-3b
tRF-5a
tRF-5b
tRF-5c
tiRNA-3
tiRNA-5
d
DA vs Normal
DA vs Normal
up_regulated tRFs & tiRNAs (14)
not differential tRFs & tiRNAs (648)
down_regulated tRFs & tiRNAs (69)
-log10(p_value)
log2(Fold Change)
f
Subtype Distribution in GROUP_ Normal
Subtype Distribution in GROUP_ DA
Number

◂**Fig. 1** Analysis of plasma tRF and tiRNA high-throughput sequencing **a**. Venn diagrams show that 240 tsRNAs were co-expressed in both groups. **b**. The Venn diagram shows the overlap number of tsRNAs found in the sequencing data and the tRFdb. **c**. Pie charts show the subtype numbers of tsRNAs in the two groups. **d**. Hierarchical clustering of the expression profile of tsRNAs in the DA and normal groups. **e**. Volcano plots of the expression profile of tsRNAs in the DA and normal groups. **f**. Stacked plots indicated the number of subtypes of tsRNAs derived from the same anti-codon tRNA in the DA and normal groups

assessed using agarose gel electrophoresis and NanoDrop ND-1000 (Thermo Fisher Scientific, Wilmington, USA). To ensure the accuracy of subsequent small RNA sequencing libraries, plasma total RNA was pretreated to eliminate potential RNA modifications. The RNA samples were then sequentially ligated to 3'and 5'adapters, reverse-transcribed, and PCR-amplified using Illumina platform-specific primers. PCR products of 134–160 bp (corresponding to 14–40 nt small RNAs) were isolated by polyacrylamide gel electrophoresis and quantified with an Agilent 2100 bioanalyzer. Libraries were denatured, diluted to 1.8 pM in 1.3 mL, and sequenced on an Illumina NextSeq 500. tsRNA sequencing was conducted with a read depth of 10 million reads per sample. The alignment rate for each sample is detailed in Supplementary Table S2. Sequencing counts were normalized to counts per million (CPM) of total aligned reads to assess tsRNA abundance.

Cell culture and transfection

NCM460 normal human colonic epithelial cells (Beina Chuanglian Biology Research Institute, China) were maintained in RPMI 1640 medium (BioInd, Israel). Other cell culture and transfection procedures were performed as previously detailed (Liu et al. 2020).

Reagents and plasmid construction

tRF-58:76-Tyr-GTA-2-M3 mimic, inhibitor and corresponding controls were procured from RIBOBIO (Guangzhou, China). Small interfering RNAs (siRNAs) targeting SUFU were synthesized by SyngenBio (Beijing, China). The 3′-untranslated region (UTR) of SUFU, including both the wild-type (WT) and a mutated (Mut) version of the predicted tRF-58:76-Tyr-GTA-2-M3 binding site, was amplified and subcloned into the pmirGLO Dual-Luciferase Vectorto generate the 3′-UTR-Luc, WT-Luc, and Mut-Luc reporters (Baihao Biological, Liaoning, China). The tRF-58:76-Tyr-GTA-2-M3 agomir and negative control were obtained from RIBOBIO.

Target gene prediction and bioinformatics analysis

Low-quality reads were filtered using the Illumina chastity filter. Clean reads were trimed and aligned to mature and precursor tRNA sequences from GtRNAdb (https://gtrnadb.ucsc.edu/) using Bowtie software (http://bowtie.cbcb.umd.edu), excluding mitochondrial tRNAs and their derivatives. The DEGseq R package was used to identify differentially expressed tsRNAs in the RNA sequencing data. Subsequent analyses, including principal component analysis (PCA), correlation analysis, pie charts, Venn charts, hierarchical clustering and volcano plots were conducted. Target genes were predicted using TargetScan 8.0 (https://www.targetscan.org/) and miRanda v6 (https://www.microRNA.org) the overlapping results were subjected to further analyses. Functional enrichment was implemented using Gene Ontology (GO) and Kyoto Encyclopedia of Genes and Genomes (KEGG) analyses via Metascape. Gene interactions were explored using GeneMANIA.

Dual-luciferase reporter assay

NCM460 cells were plated in 24-well plates and transfected at 70–80% confluence. The SUFU 3′-UTR sequences containing the predicted tRF-58:76-Tyr-GTA-2-M3 binding sites were cloned into the pmirGLO dual-luciferase vector (Promega, Madison, WI, USA). 24 h later, luciferase reporter gene plasmid and tRF-58:76-Tyr-GTA-2-M3 mimic/mimic NC were transfected. Following a 48-h incubation, Luciferase activity was detected using the Dual-Luciferase Reporter Assay System (Promega) and quantified by a Tecan Infinite M200 Pro Multimode Reader.

Reverse transcription and qRT-PCR

The details can be found in our previous study (Liu et al. 2020). Primers for tsRNA and mRNA were synthesized by RIBOBIO, and Sangon Biotech,

respectively (sequence listed in Supplementary Table S3). U6 and β-actin served as internal controls.

Hematoxylin and eosin staining (HE)

Fresh fetal duodenum tissue from ARM was harvested and processed for HE. Further details referred to our previous study (Liu et al. 2020).

TUNEL assay

The TUNEL assay was conducted using an in situ cell death detection kit (Roche, Mannheim, Germany), according to the manufacturer's instructions. The details can be found in our previous study (Huang et al. 2021).

Fluorescence in situ hybridization (FISH)

FISH was conducted using a tRF-58:76-Tyr-GTA-2-M3 probe designed and synthesized by ServiceBio (Wuhan, China). TUNEL-stained sections were pre-hybridized at 37 °C for 1 h, Followed by hybridization with the probe solution overnight at 40 °C. After washing, sections were incubated with pre-warmed Probe Mix 2 at 40 °C for 45 min. Nuclei were counterstained with DAPI and incubated in the dark for eight minutes. After rinsing and mounting with anti-fluorescence quenching retardant, images were captured using a confocal microscope. TUNEL-positive (green) and FISH -positive (red) cells were subsequently quantified.

Western blotting

Proteins were extracted from NCM460 cells or duodenum tissue. Western blotting was performed according to previous study (Liu et al. 2020). All the antibody information is presented in Supplementary Table S4.

Flow cytometry assay

Cellular apoptosis was assessed using an Annexin V-FITC/propidium iodide double staining kit (Vazyme Biotech, Nanjing) and quantified by flow cytometry (BD Biosciences).

Intraperitoneal microinjection

Pregnant rats were administered 1% adriamycin and anesthetized with 2–5% isoflurane (RWD, Shenzhen, China) on E16. Following a mid-lower abnormal incision, the uterus was exteriorized, covered with moist gauze, and placed in warm saline. Fetal rats were randomly assigned to receive either 5 μL of PBS (n = 46) or 5 μL of tRF-58:76-Tyr-GTA-2-M3 agomir (n = 59) via intraperitoneal injection through the uterine wall using a micro-injection pump (RWD) and a glass capillary needle. Injection was performed on the ventral side to avoid placenta and umbilical cord injury. After injection, the uterus was repositioned and the abdominal wall was sutured. On E21, pregnant rats were euthanized, and fetuses were harvested and captured by a Leica fluorescence stereomicroscope.

Statistical analysis

Statistical analyses were performed using GraphPad Prism V. 8 (GraphPad, La Jolla, USA) and SPSS Statistics V. 26 (IBM, Armonk, USA). Data are presented as mean ± standard deviation (SD) for normal distributed variables or median (interquartile range) for non-normally distributed variables. The normality of variance distribution and homogeneity was evaluated before data analysis. Comparisons between two groups were conducted using the unpaired t-test or Mann–Whitney test, as appropriate. For multiple group comparisons, one-way ANOVA with Turkey's or Dunnett's post hoc test was applied. Paired t-test or Wilcoxon test were used to compare tsRNA expression between 38–40 weeks of gestation and 24 h after delivery. Chi-square test was used to analyze differences in DA and type III DA rates among control, PBS, and tRF-58:76-Tyr-GTA-2-M3 agomir groups. The area under the receiver operating characteristic (ROC) curve (AUC) was calculated using MedCalc 19.0.7 to assess the diagnostic potential of the tsRNAs. Statistical significance was defined as $*P < 0.05$ and $**P < 0.01$.

Results

Overview of tsRNAs profiling in plasma

To investigate and characterize the differentially expressed tsRNAs in the maternal plasma of DA, we

analyzed tsRNA expression profiles in three pairs of maternal plasma from DA and matched maternal plasma from normal fetuses using high-throughput sequencing technology. A total of 731 tsRNAs were identified using tRF and tiRNA sequencing. Venn diagram analysis indicated that 240 tsRNAs were co-expressed in both groups, and 85 tsRNAs were identified from the sequencing results and validated using tRFdb (a database for the transfer of RNA fragments) (Fig. 1a-b). Component analysis revealed remarkable changes in the expression levels of tsRNAs across subtypes. The distribution of tsRNAs across subtypes in the maternal plasma of both normal and DA groups was primarily represented by tRF-3 and tRF-5 (Fig. 1c). Subsequently, we applied filter conditions of fold change > 1.5 and $P < 0.05$, which resulted in the identification of 83 differentially expressed tsRNAs, of which 14 were upregulated and 69 were downregulated (Fig. 1d-e). This indicated that the number of downregulated tsRNAs was significantly greater than upregulated tsRNAs, with the fold change in downregulation being substantially higher than that in upregulation. The stacked plots demonstrate the quantity of tsRNAs derived from tRNAs with identical amino acids and anticodons in the normal and DA groups following the removal of redundant data. tRNA-Gly-GCC was responsible for generating the highest number of tsRNAs in both groups (Fig. 1f).

qRT-PCR verification of three pairs of original sequencing samples

Most differentially expressed tsRNAs were downregulated, with the fold change of the downregulated tsRNAs exceeding that of the upregulated tsRNAs by a significant margin. To validate the tRF and tiRNA sequencing results, we initially selected the top 10 tsRNAs exhibiting the greatest downregulation and subsequently validated them in three pairs of original sequencing samples. A comprehensive account of the differentially expressed tsRNAs is presented in Supplementary Table S5. The expression levels of these 10 candidate tsRNAs were assessed using qRT-PCR (Supplementary Fig. S2). Among them, seven tsRNAs exhibite significant downregulation in the DA maternal plasma of the original sequencing samples ($P < 0.05$), which were consistent with those of sequencing. These included tRF-69:85-Ser-GCT-3-M4, tRF-61:78-chrM. Leu-TAA, tRF-60:77-Ile-AAT-1-M4, tRF-57:76-Arg-ACG-1-M2, tRF-58:76-Tyr-GTA-2-M3, tRF-68:85-Ser-TGA-4, and tRF-70:86-Leu-CAG-1.

qRT-PCR analysis of 35 paired plasma samples in the validation phase of the study

The seven tsRNAs initially identified by sequencing were subsequently evaluated using qRT-PCR. As illustrated in Fig. 2a, four tsRNAs were identified: tRF-61:78-chrM. Leu-TAA, tRF-60:77-Ile-AAT-1-M4, tRF-57:76-Arg-ACG-1-M2, and tRF-58:76-Tyr-GTA-2-M3 were significantly dysregulated in the plasma samples of pregnant women carrying fetuses with DA compared with those carrying normal fetuses ($P < 0.05$). The diagnostic value of tRF-61:78-chrM.Leu-TAA, tRF-60:77-Ile-AAT-1-M4, tRF-57:76-Arg-ACG-1-M2, and tRF-58:76-Tyr-GTA-2-M3 for fetal DA was assessed using ROC curve analysis of 35 case–control pairs. The results indicated high diagnostic accuracy for these tsRNAs, with AUCs of 0.728, 0.738, 0.731, and 0.748, respectively ($P < 0.001$). The sensitivity and specificity were as follows: tRF-61:78-chrM.Leu-TAA: 58.33% sensitivity, 83.36% specificity; tRF-60:77-Ile-AAT-1-M4: 61.11% sensitivity, 83.33% specificity; tRF-57:76-Arg-ACG-1-M2: 77.78% sensitivity, 63.89% specificity; tRF-58:76-Tyr-GTA-2-M3: 48.57% sensitivity, 91.43% specificity (all $P < 0.001$). Furthermore, the combination of these four tsRNAs yielded an AUC of 0.798, with a sensitivity of 48.57% and specificity of 88.57% (Fig. 2b and Supplementary Table S6).

tsRNAs expression in plasma from women with normal fetuses before and after delivery and in plasma samples from women with other types of gastrointestinal atresia

The current research aimed to ascertain whether the expression of four candidate tsRNAs are correlated with pregnancy. Plasma levels were validated using qRT-PCR at 38–40 weeks of gestation and 24 h after normal delivery in 17 pregnant women (Fig. 3a). 24 h after delivery, tsRNA expression levels always decreased. Therefore, it has been speculated that the four tsRNAs were associated with pregnancy. Furthermore, the potential of these four tsRNAs as molecular markers for the prenatal diagnosis of other types of gastrointestinal atresia, specifically EA and

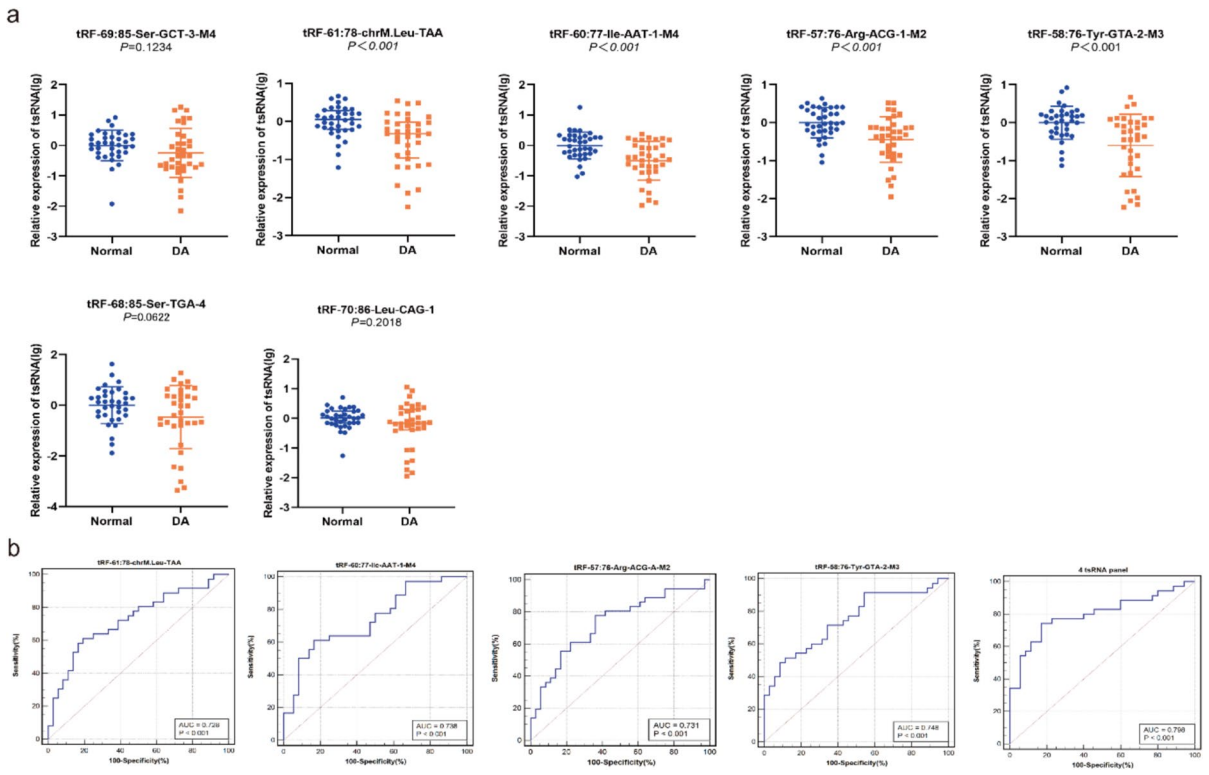

Fig. 2 Relative expression of the seven tsRNAs in the plasma of pregnant women carrying DA and normal fetuses. **a**. qRT-PCR analysis was performed on the 35 paired plasma from pregnant women carrying fetuses with DA (n = 35) and pregnant women carrying normal fetuses (n = 35). U6 was used as an internal control. *P* values were determined using unpaired t-test for normally distributed data and Mann–Whitney U test for nonparametric data. qRT-PCR measurements were performed in duplicate. Data are expressed as mean ± SD (unpaired t-test) or median and interquartile range (Mann–Whitney test). **b**. ROC curves of four differentially expressed tsRNAs and a combination of the four tsRNAs in plasma from 35 case–control pairs (normal group, n = 35; DA group, n = 35)

JIA, was investigated. The results demonstrated that tRF-61:78-chrM. Leu-TAA, tRF-60:77-Ile-AAT-1-M4, tRF-57:76-Arg-ACG-1-M2, and tRF-58:76-Tyr-GTA-2-M3 were significantly reduced in the plasma of pregnant women with EA (Fig. 3b). However, no difference was observed in the plasma of pregnant women with JIA (Fig. 3c). Thus, it can be concluded that these four tsRNAs may have diagnostic value for EA, and further validation with a larger sample size is required.

tRF-58:76-Tyr-GTA-2-M3 is downregulated in fetal duodenum of DA and inhibited apoptosis in NCM460 cells

Among the four tsRNA biomarkers, tRF-58:76-Tyr-GTA-2-M3 demonstrated the most significant area under the ROC curve and highest diagnostic accuracy. Therefore, we focused our efforts on tRF-58:76-Tyr-GTA-2-M3 to ascertain its potential involvement in the pathogenesis of DA. According to the MINIbase v2.0 database, tRF-58:76-Tyr-GTA-2-M3 is derived from the 3'end of the mature tRNA-Tyr-GTA and comprises 19 bases, with a sequence of 5'-Attccggctcgaaggacca-3'and a shear site located in the T-Loop (TTCGATT) (Fig. 4a). Furthermore, four paired duodenal specimens were collected from fetuses with DA and normal fetuses; their clinical characteristics are presented in Supplementary Table S7. The expression of tRF-58:76-Tyr-GTA-2-M3 in the duodenum of fetuses with DA was markedly diminished, which correlated with the expression observed in the plasma of pregnant women with DA (Fig. 4b). To investigate the role of apoptosis in the

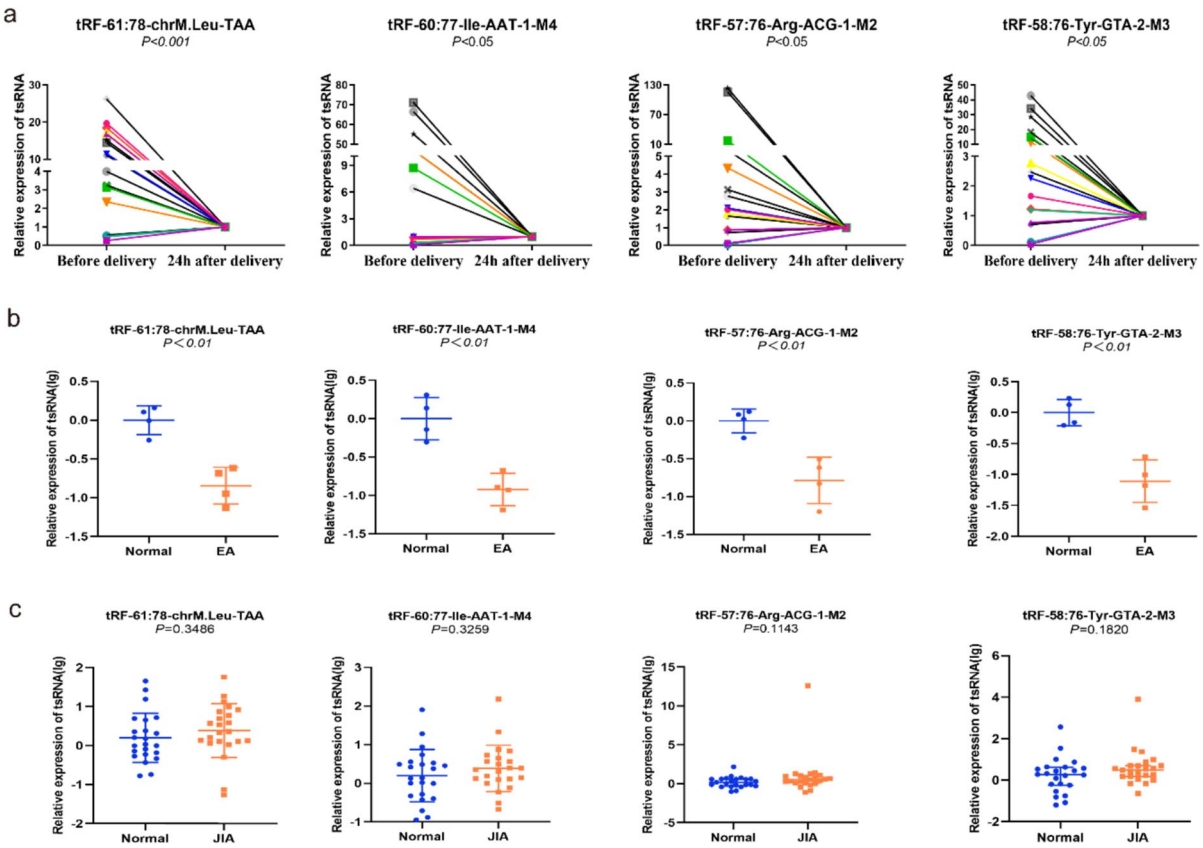

Fig. 3 qPCR analysis of tsRNAs during the additional validation phase. **a**. Scatter plots of tRF-61:78-chrM.Leu-TAA, tRF-60:77-Ile-AAT-1-M4, tRF-57:76-Arg-ACG-1-M2, and tRF-58:76-Tyr-GTA-2-M3. Each line represents one plasma sample from the same pregnant woman at 38–40 weeks of gestation and 24 h after delivery (n = 17). P value was determined by paired t-test for normally distributed data, and paired Wilcoxon test for non-parametric data. **b**. Relative tsRNAs expression of tRF-61:78-chrM.Leu-TAA, tRF-60:77-Ile-AAT-1-M4, tRF-57:76-Arg-ACG-1-M2, and tRF-58:76-Tyr-GTA-2-M3 in pregnant women with EA (n = 4) and normal fetuses (n = 4). **c**. Relative tsRNA expression in tRF-61:78-chrM. Leu-TAA, tRF-60:77-Ile-AAT-1-M4, tRF-57:76-Arg-ACG-1-M2, and tRF-58:76-Tyr-GTA-2-M3 in pregnant women with JIA (n = 23) and in normal fetuses (n = 23). U6 was used as an internal control. *P* value was determined using unpaired t-test for normally distributed data and Mann–Whitney U test for nonparametric data

formation of DA, the expression of apoptosis-related markers in the duodenum of fetal DA was detected. As illustrated in Fig. 4c, the expression levels of Cleaved-Caspase-3 and the BAX/BCL2 ratio in the fetal duodenal tissue of the DA group were remarkably higher than those in the normal group, indicating that an increase in apoptosis contributed to the occurrence of DA.

To ascertain whether tRF-58:76-Tyr-GTA-2-M3 plays a role in the pathogenesis of DA by influencing apoptosis, we conducted a series of transfections of NCM460 cells. The transfections involved the use of a tRF-58:76-Tyr-GTA-2-M3 mimic, tRF-58:76-Tyr-GTA-2-M3 inhibitor, and their corresponding negative controls (sequences are provided in Supplementary Table S8). The transfection efficiency of tRF-58:76-Tyr-GTA-2-M3 was initially validated, and it was observed that the expression levels were markedly elevated following the transfection of the tRF-58:76-Tyr-GTA-2-M3 mimic into NCM460 cells (Supplementary Fig. S3). TUNEL staining was performed, and BAX, BCL2, and Caspase-3 expression was quantified in NCM460 cells following transfection with the tRF-58:76-Tyr-GTA-M3 mimic and NC. Transfection with the tRF-58:76-Tyr-GTA-M3 mimic resulted in

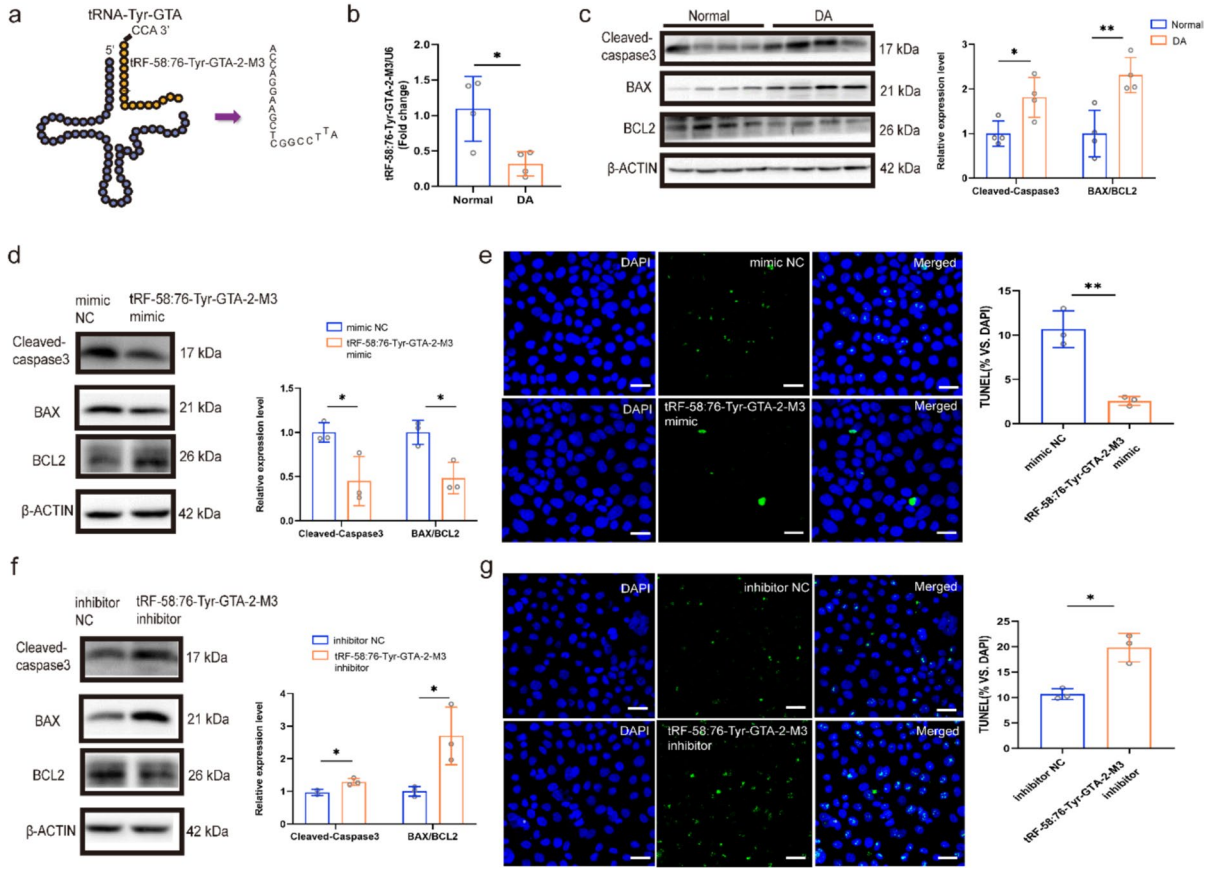

Fig. 4 tRF-58:76-Tyr-GTA-2-M3 is downregulated in the fetal duodenum of DA and mediated apoptosis of NCM460 cells. **a**. Shear position and sequence of tRF-58:76-Tyr-GTA-2-M3. **b**. qPCR analysis of tRF-58:76-Tyr-GTA-2-M3 expression in the duodenum of DA and normal fetuses. U6 was used as an internal control. Data are presented as the mean ± SD (n = 4, $*P < 0.05$; Unpaired t-test). **c**. The expression of apoptosis-related proteins in the duodenum of DA and normal fetuses. Data are presented as the mean ± SD (n = 4, $*P < 0.05$, $**P < 0.01$; Unpaired t-test). **d**. Apoptosis-related proteins (Cleaved-Caspase-3, BAX and BCL2) were detected using western blotting in NCM460 cells transfected with an tRF-58:76-Tyr-GTA-M3 mimic or a mimic NC. Data are presented as the mean ± SD (n = 3, $*P < 0.05$; Unpaired t-test). **e**. TUNEL assay showing representative confocal microscopic images of apoptotic NCM460 cells transfected with an tRF-58:76-Tyr-GTA-M3 mimic or a mimic NC, and the number of TUNEL-positive cells was counted in each field at 200 × magnification, scale bar = 10 μm (n = 3, $**P < 0.01$; Unpaired t-test). **f**. Apoptosis-related proteins (Cleaved-Caspase-3, BAX, and BCL2) were detected by western blotting in NCM460 cells transfected with a tRF-58:76-Tyr-GTA-M3 inhibitor or NC inhibitor (n = 3, $*P < 0.05$; Unpaired t-test). **g**. TUNEL assay showing representative confocal microscopic images of apoptotic NCM460 cells transfected with an tRF-58:76-Tyr-GTA-M3 inhibitor or an inhibitor NC, and the number of TUNEL-positive cells was counted in each field at 200 × magnification, scale bar = 10 μm (n = 3, $*P < 0.05$; Unpaired t-test)

downregulation of the pro-apoptotic proteins Caspase-3 and BAX, accompanied by upregulation of the anti-apoptotic protein BCL2 (Fig. 4d). Consistently, TUNEL assay revealed a marked decrease in apoptotic cell numbers in NCM460 cells transfected with the tRF-58:76-Tyr-GTA-M3 mimic compared to the negative control (Fig. 4e). In contrast, transfectants of the tRF-58:76-Tyr-GTA-M3 inhibitor exhibited augmented apoptosis, as evidenced by the TUNEL assay and elevated expression of Caspase-3 and BAX/BCL2 ratio (Fig. 4f-g).

tRF-58:76-Tyr-GTA-2-M3 directly targeted SUFU

The target genes of tRF-58:76-Tyr-GTA-2-M3 were predicted using TargetScan 8.0 and miRanda v6, and subsequently classified through GO and KEGG pathway analyses. A total of 334 target genes were

identified, most which were associated with biological processes related to embryonic development. These processes included embryonic morphogenesis, cardiac chamber development, telencephalon development, embryonic limb development, and the positive regulation of mesenchymal cell apoptosis (Fig. 5a). The results of the KEGG pathway analysis are presented in Supplementary Fig. S4. The GeneMANIA network revealed potential interactions among the predicted target genes (Fig. 5b). We observed over three instances of gene intersections across these five categories. Based on these observations, we selected eight candidate target genes (*TBX2*, *ID3*, *HOXA3*, *HOXA13*, *FOXE1*, *HDAC2*, *FZD2*, and *SUFU*) for further validation. qRT-PCR revealed that *SUFU* mRNA expression in the fetal duodenum of the DA group was markedly elevated compared with that in the normal group ($P < 0.01$), indicating a potential inverse regulatory relationship with tRF-58:76-Tyr-GTA-2-M3 (Fig. 5c). Furthermore, the expression level of SUFU protein in fetal duodenal tissue was quantified, revealing a significant upregulation of SUFU in DA fetal duodenal tissue (Fig. 5d). To confirm the direct relationship between tRF-58:76-Tyr-GTA-2-M3 and *SUFU*, a dual-luciferase vector was constructed to clone the 3′-UTR of *SUFU*. The bioinformatics databases TargetScan and miRanda indicated that *SUFU* contains a binding site for tRF-58:76-Tyr-GTA-2-M3 (Fig. 5e). Subsequently, a luciferase assay was conducted by co-transfecting tRF-58:76-Tyr-GTA-2-M3 mimic and NC with Luc-SUFU into NCM460 cells. Compared to the control group, the tRF-58:76-Tyr-GTA-2-M3 mimic resulted in a reduction in Luc-SUFU luciferase reporter activity (Fig. 5f). The regulatory relationship between tRF-58:76-Tyr-GTA-2-M3 and *SUFU* expression was also investigated. As illustrated in Fig. 5g-h, SUFU RNA and protein expression levels decreased in the tRF-58:76-Tyr-GTA-2-M3 mimic group and increased in the tRF-58:76-Tyr-GTA-2-M3 inhibitor group.

SUFU regulated apoptosis and increased GLI1 expression levels

SUFU functions as a negative regulator of the hedgehog signaling pathway by interacting with GLI1, a pivotal transcription factor within this pathway, to impede GLI1 nuclear translocation and, consequently, the suppression of hedgehog signaling (He et al. 2020; Zhang et al. 2017). We further detected the expression levels of GLI1 in the fetal duodenum of DA. Figure 6a illustrates that the expression level of GLI1 protein in the lesion tissue was diminished, suggesting that the hedgehog signaling pathway may be inhibited during the formation of DA. Subsequently, NCM460 cells were transfected with tRF-58:76-Tyr-GTA-2-M3 mimic and inhibitor. The results demonstrated that GLI1 protein expression was markedly elevated following transfection with the tRF-58:76-Tyr-GTA-2-M3 mimic, whereas it was significantly reduced following transfection with the tRF-58:76-Tyr-GTA-2-M3 inhibitor (Fig. 6b). To further elucidate the impact of SUFU on embryogenesis through apoptosis and its biological function in regulating GLI1 expression, we quantified the expression of apoptosis-related proteins in NCM460 cells following transfection with small interfering RNAs (siRNAs). Three siRNAs targeting SUFU mRNA (Supplementary Table S9) were designed and evaluated for their silencing efficiency. Among them, siSUFU#1 exhibited the most potent suppression of both SUFU mRNA and protein expression levels (Fig. 6c–d), and was selected for use in subsequent research. Therefore, si SUFU#1 was selected for the subsequent experiments. The use of si SUFU#1 resulted in increased GLI1 levels and decreased Cleaved-Caspase-3 and BAX: BCL2 ratio in NCM460 cells (Fig. 6e). To ascertain whether the effects of the tRF-58:76-Tyr-GTA-2-M3 inhibitor could be counteracted by si SUFU#1, we co-transfected NCM460 cells with tRF-58:76-Tyr-GTA-2-M3 inhibitor and si SUFU#1. The results demonstrated that the upregulation of SUFU and downregulation of GLI1 induced by tRF-58:76-Tyr-GTA-2-M3 knockdown was partially reversed by si SUFU#1. Moreover, si SUFU#1 partially attenuated apoptosis induced by tRF-58:76-Tyr-GTA-2-M3 inhibition, as evidenced by flow cytometry (Fig. 6f-g). In conclusion, these findings collectively indicate that tRF-58:76-Tyr-GTA-2-M3 influences apoptosis in NCM460 cells through the modulation of SUFU and GLI1 expression.

The expression of tRF-58:76-Tyr-GTA-2-M3, Sufu, Gli1 and apoptosis-related proteins in duodenum of ARM

The duodenum of the fetal rats was meticulously identified and isolated under a stereomicroscope.

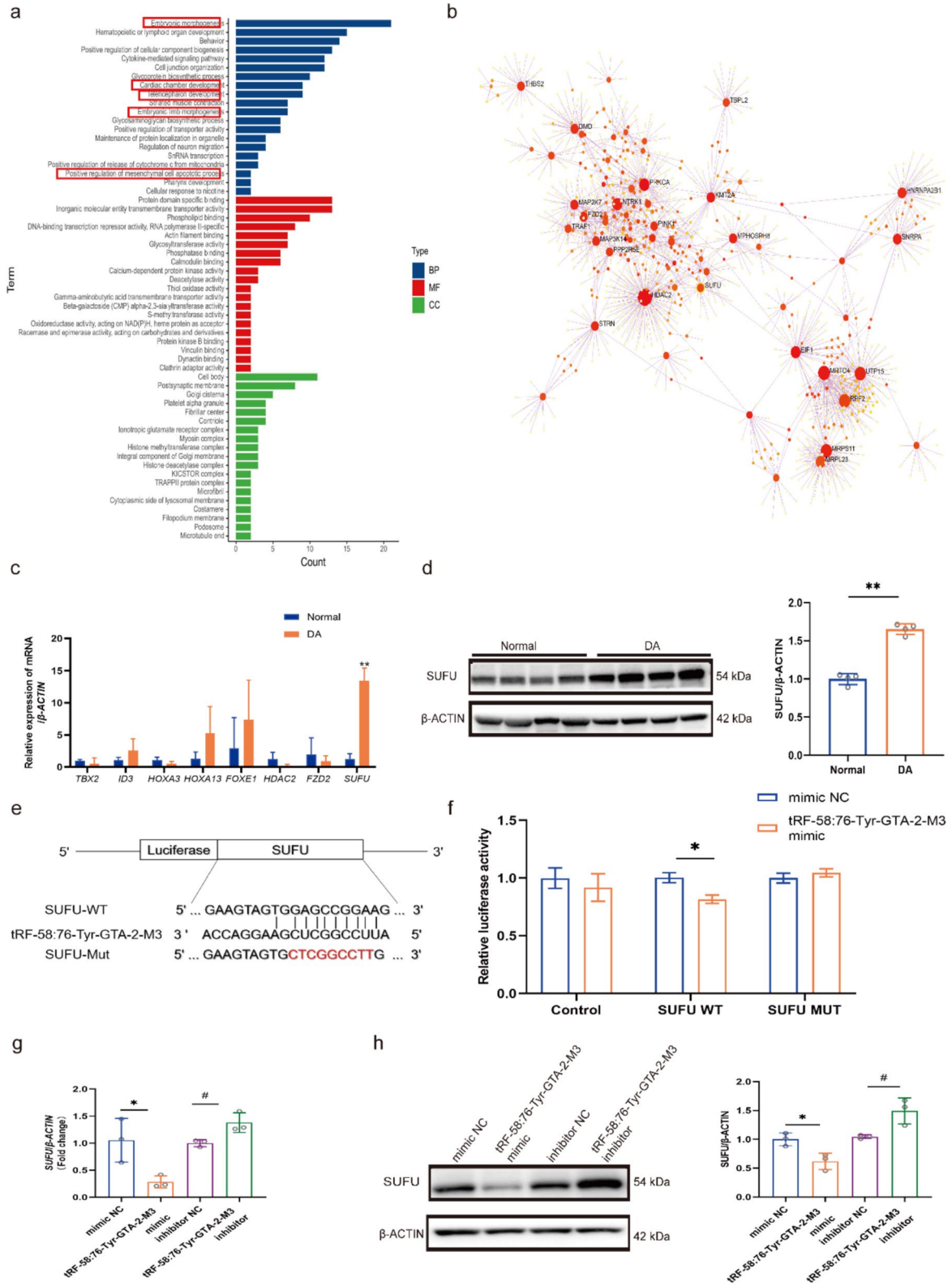
a
Term
Count
Type
BP
MF
CC
b
c
Normal
DA
Relative expression of mRNA /β-ACTIN
TBX2
ID3
HOXA3
HOXA13
FOXE1
HDAC2
FZD2
SUFU
d
Normal
DA
SUFU
β-ACTIN
54 kDa
42 kDa
SUFU/β-ACTIN
e
5'
Luciferase
SUFU
3'
SUFU-WT 5' ... GAAGTAGTGGAGCCGGAAG ... 3'
tRF-58:76-Tyr-GTA-2-M3 3' ACCAGGAAGCUCGGCCUUA 5'
SUFU-Mut 5' ... GAAGTAGTGCTCGGCCTTG ... 3'
f
mimic NC
tRF-58:76-Tyr-GTA-2-M3 mimic
Relative luciferase activity
Control
SUFU WT
SUFU MUT
g
SUFU/β-ACTIN (Fold change)
mimic NC
tRF-58:76-Tyr-GTA-2-M3 mimic
inhibitor NC
tRF-58:76-Tyr-GTA-2-M3 inhibitor
h
mimic NC
tRF-58:76-Tyr-GTA-2-M3 mimic
inhibitor NC
tRF-58:76-Tyr-GTA-2-M3 inhibitor
SUFU
β-ACTIN
54 kDa
42 kDa
SUFU/β-ACTIN

◂**Fig. 5** *SUFU* is a target gene of tRF-58:76-Tyr-GTA-2-M3. **a**. GO enrichment analysis was performed to show enrichment classification information for target genes of tRF-58:76-Tyr-GTA-2-M3 (https://metascape.org/gp/index.html). **b**. GeneMANIA network of the predicted target genes (htttps://Genemania.org). **c**. qRT-PCR of the eight candidate target genes (*TBX2*, *ID3*, *HOXA3*, *HOXA13*, *FOXE1*, *HDAC2*, *FZD2*, *SUFU*) in duodenum of DA fetuses and normal fetuses. β-ACTIN as an endogenous control. Data are presented as the mean ± SD (n = 4, $^{**}P < 0.01$; Unpaired t-test). **d**. Western blot analysis for SUFU expression in duodenum of DA fetuses and normal fetuses. β-ACTIN as an endogenous control. Data are presented as the mean ± SD (n = 4, $^{**}P < 0.01$; Unpaired t-test). **e**. Predicted tRF-58:76-Tyr-GTA-2-M3 binding site in SUFU (SUFU-WT) and the designed mutant sequence (SUFU-Mut). **f**. Luciferase reporter assay of NCM460 cells co-transfected with SUFU-WT or SUFU-Mut and tRF-58:76-Tyr-GTA-2-M3 mimic or tRF-58:76-Tyr-GTA-2-M3 mimic NC. Data are presented as the mean ± SD (n = 3, $^{*}P < 0.05$; Unpaired t-test). **g**. Relative SUFU mRNA expression in NCM460 cells transfected with tRF-58:76-Tyr-GTA-2-M3 mimic, tRF-58:76-Tyr-GTA-2-M3 inhibitor and their corresponding NC measured by qRT-PCR. β-ACTIN as an endogenous control. Data are presented as the mean ± SD ($^{*}P < 0.05$ relative to the mimic NC group, $\#P < 0.05$ relative to the inhibitor NC group; Unpaired t-test). **h**. Relative SUFU protein expression in NCM460 cells transfected with tRF-58:76-Tyr-GTA-2-M3 mimic, tRF-58:76-Tyr-GTA-2-M3 inhibitor, and their corresponding NC measured by western blotting. β-ACTIN as an endogenous control. Data are presented as the mean ± SD ($^{*}P < 0.05$ relative to the mimic NC group, $\#P < 0.05$ relative to the inhibitor NC group; Unpaired t-test)

Subsequently, the duodenum was stained with HE, revealing three morphological types of DA, consistent with descriptions reported in the literature (Jones et al. 2020). These reflect more serious degrees of obstruction and discontinuity, ranging from Type I to Type III (Fig. 7a-b). To ensure the reliability of specimen collection, only duodenal samples from Type III were selected for validation experiments. Fifteen pregnant rats were assigned to the E17 DA group, 16 to the E19 DA group, and 14 to the E21 DA group. Furthermore, specimens were collected from 10 pregnant rats at E17, E19, and E21, which served as control. The incidence of DA in ARM is presented in Supplementary Table S10, and the number of fetal rats collected at each time point is shown in Supplementary Table S11. To further investigate the expression of tRF-58:76-Tyr-GTA-2-M3 during embryonic development, we used qRT-PCR to assess the expression levels of tRF-58:76-Tyr-GTA-2-M3 in the duodenum of fetal DA rats at different gestational ages. The results demonstrated that tRF-58:76-Tyr-GTA-2-M3 was markedly reduced in the duodenum of the DA group at various stages of embryonic development compared to the control group, with the most notable difference observed at E17. In the duodenum of normal rat fetuses, the expression of tRF-58:76-Tyr-GTA-2-M3 exhibited a time-dependent pattern, with a decrease observed with advancing gestational age (Fig. 7c). Furthermore, in the duodenum of E19 fetal rats, the expression of the Sufu protein was increased, whereas the expression of Gli1 protein was decreased, and there was an increase in apoptosis (Fig. 7d-f).

Excessive apoptosis was ameliorated through the activation of the Hedgehog signaling pathway following intraperitoneal microinjection of tRF-58:76-Tyr-GTA-2-M3

To investigate whether upregulation of tRF-58:76-Tyr-GTA-2-M3 during embryogenesis could attenuate excessive apoptosis via activation of the Hedgehog signaling pathway. tRF-58:76-Tyr-GTA-2-M3 agomir was injected intraperitoneally into fetal rats with DAs at E16 (Fig. 8a). On E21, fetal rats with DAs that had been treated with tRF-58:76-Tyr-GTA-2-M3 were harvested. Of the 59 fetal rats that received an intraperitoneal microinjection of tRF-58:76-Tyr-GTA-2-M3 agomir at E16, 39 survived. Of the total number of rats, 18 were identified as DA fetal rats (46.2%, 18/39), comprising 1 type I, 4 type II, and 13 type III rats. Furthermore, 46 fetal rats were subjected to intraperitoneal microinjection of PBS, of which 39 survived, resulting in 30 DA fetal rats (76.9%, 30/39). This group comprised 0 type I, 1 type II, and 29 type III rats. A total of 39 normal fetal rats were obtained from control pregnant rats, and no malformations were observed. The incidence and classification of DA in fetal rats across each group are shown in Fig. 8b-c, respectively. Following intraperitoneal injection of tRF-58:76-Tyr-GTA-2-M3 agomir, the rate of DA in fetal rats was remarkable reduced compared to that observed in the control group, with a notably lower incidence of type III DA. In addition, duodenal specimens of fetal rats from each treatment group were collected, and the expression of tRF-58:76-Tyr-GTA-2-M3 in samples from each group was assessed using qRT-PCR. The expression of Sufu, Gli1, and apoptosis-related proteins in the samples from each group was analyzed by western blotting. As illustrated in Fig. 8d, the expression of

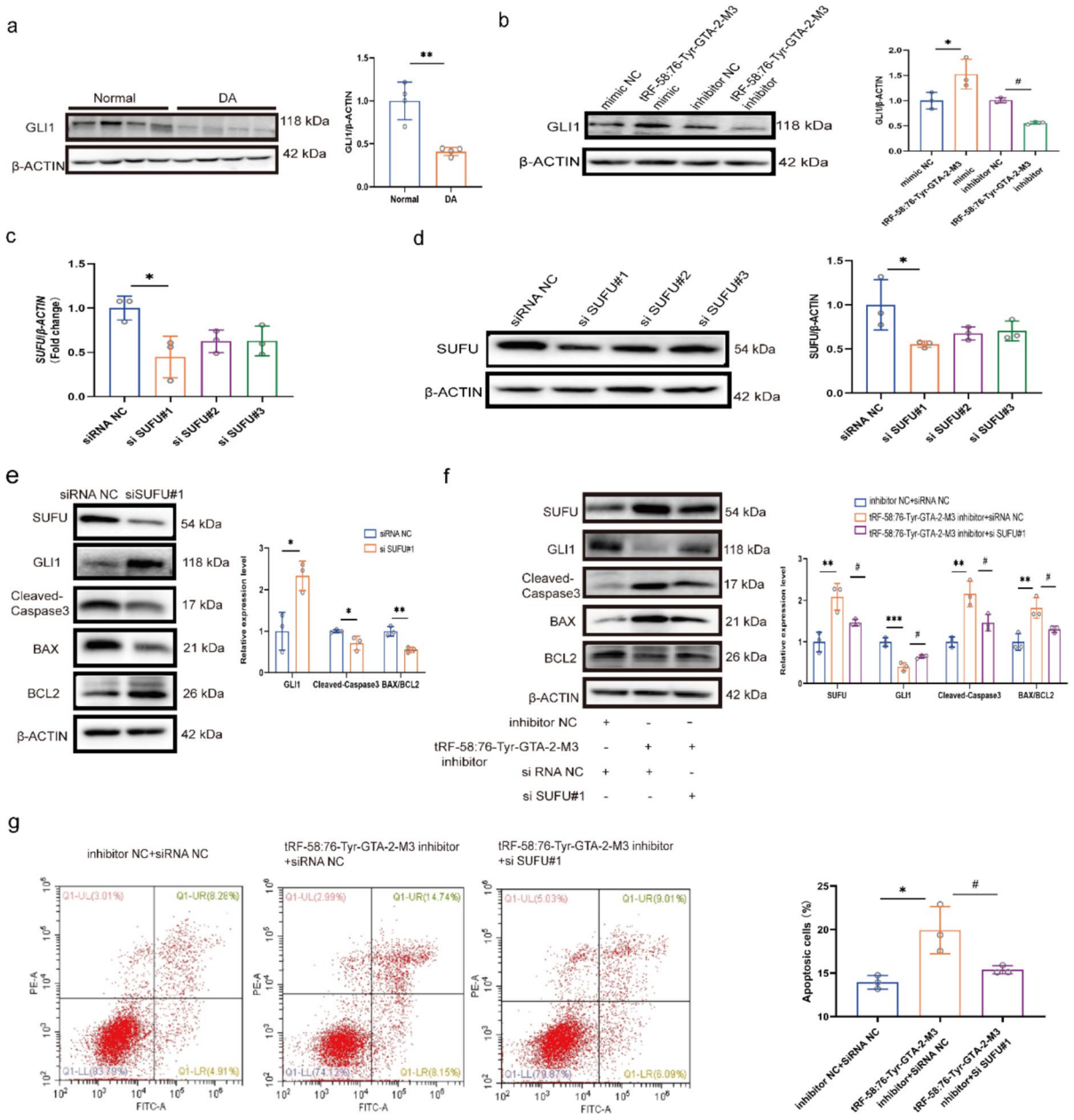

tRF-58:76-Tyr-GTA-2-M3 in the duodenum of fetal rats in the ARM group was markedly diminished compared to that in the control group. Conversely, administration of tRF-58:76-Tyr-GTA-2-M3 agomir resulted in a notable elevation in tRF-58:76-Tyr-GTA-2-M3 expression levels in the ARM group. Western blot demonstrated that the levels of Sufu, Cleaved Caspase-3, and Bax were elevated, whereas those of Gli1 and Bcl-2 were markedly diminished in the ARM group. Specifically, Sufu, Cleaved Caspase-3, and Bax protein expression were markedly reduced, whereas Gli1 and Bcl-2 expression were significantly elevated in the duodenum of fetal rats (Fig. 8e). To ascertain the relationship between tRF-58:76-Tyr-GTA-2-M3 expression and apoptosis in the duodenum of each treatment group, FISH and TUNEL double staining were performed. As illustrated in Fig. 8f, the expression of tRF-58:76-Tyr-GTA-2-M3 was

◂**Fig. 6** SUFU regulates apoptosis and increases GLI1 expression in NCM460 cells. **a**. Western blot analysis for GLI1 expression in duodenum of DA fetuses and normal fetuses. β-ACTIN as an endogenous control. Data are presented as the mean ± SD (n = 4, $^{**}P < 0.01$; Unpaired t-test). **b**. Relative SUFU protein expression in NCM460 cells transfected with tRF-58:76-Tyr-GTA-2-M3 mimic, tRF-58:76-Tyr-GTA-2-M3 inhibitor, and their corresponding NC measured by western blotting. β-ACTIN as an endogenous control. Data are presented as the mean ± SD (n = 3, $^{*}P < 0.05$ relative to the mimic NC group, $\#P < 0.05$ relative to the inhibitor NC group; Unpaired t-test). **c**-**d**. RNA and protein levels of *SUFU* in NCM460 cells transfected with si SUFU#1 or NC for 48 h. β-ACTIN as an endogenous control. Data are presented as the mean ± SD (n = 3, $^{*}P < 0.05$; relative to the NC group; one-way ANOVA with Dunnett correction). **e**. Relative SUFU, GLI1, Cleaved-Caspase3, BAX and BCL2 protein expression in NCM460 cells transfected with si SUFU#1 and its NC measured by Western blot. β-ACTIN as an endogenous control. Data are presented as the mean ± SD (n = 3, $^{*}P < 0.05$, $^{**}P < 0.01$; Unpaired t-test). **f**. NCM460 cells were co-transfected with inhibitor NC + siRNA NC or tRF-58:76-Tyr-GTA-2-M3 inhibitor + siRNA NC or tRF-58:76-Tyr-GTA-2-M3 inhibitor + si SUFU#1, and the expression levels of SUFU and GLI1 proteins and apoptosis-related proteins were detected by Western blot. β-ACTIN as an endogenous control. Data are presented as the mean ± SD (n = 3, $^{**}P < 0.01$ relative to inhibitor NC + siRNA NC group, $^{***}P < 0.001$ relative to inhibitor NC + siRNA NC group, #P < 0.05 relative to tRF-58:76-Tyr-GTA-2-M3 inhibitor + siRNA NC group; one-way ANOVA with Turkey correction). **g**. The apoptotic ability of the co-transfected cells was detected using flow cytometry. Data are presented as the mean ± SD (n = 3, $^{*}P < 0.05$ relative to inhibitor NC + siRNA NC group, $\#P < 0.05$ relative to tRF-58:76-Tyr-GTA-2-M3 inhibitor + siRNA NC group; one-way ANOVA with Turkey correction)

lower in the ARM group than in the control group, accompanied by a significant increase in the number of apoptotic cells. In contrast, the malformation group treated with the tRF-58:76-Tyr-GTA-2-M3 agomir exhibited elevated expression of tRF-58:76-Tyr-GTA-2-M3 and a remarkable reduction in the number of apoptotic cells. In conclusion, these findings suggest that intraperitoneal microinjection of tRF-58:76-Tyr-GTA-2-M3 agomir can attenuate apoptosis in fetal rat duodenum with DA by regulating the expression of Sufu and Gli1.

Discussion

The exploration of nucleic acids in blood circulation and other bodily fluids as non-invasive biomarkers for congenital malformations screening has recently garnered increasing attention in the scientific community. By conducting proteomic, transcriptomic, and lipidomic screening of maternal peripheral blood and subsequently validating the results through the use of expanded sample sizes, our research group has identified specific proteins, piRNAs, and miRNAs with diagnostic value in screening for congenital heart disease, neural tube defects, and non-syndromic cleft lip and palate (An et al. 2015; Chen et al. 2016; Dong et al. 2020; Gu et al. 2019, 2012; Jia et al. 2021; Wang et al. 2022). tsRNAs emerge as a promising class of clinical biomarkers due to their high specificity and stability. In this study, we revealed for the first time that tsRNAs in maternal plasma can serve as biomarkers for prenatal diagnosis of DA, offering the potential for non-invasive prenatal diagnosis. Through high-throughput sequencing of tRF and tiRNA, and subsequent validation by qRT-PCR of the maternal plasma, we identified tRF-61:78-chrM. Leu-TAA, tRF-60:77-Ile-AAT-1-M4, tRF-57:76-Arg-ACG-1-M2, and tRF-58:76-Tyr-GTA-2-M3 were expressed at low levels in the maternal plasma of pregnant women carrying DA, and may serve as candidate biomarkers for prenatal screening of DA. ROC curve analysis showed these markers exhibited high specificity for DA screening and that the combination of the four tsRNAs enhanced their diagnostic efficiency. The specificity of these tsRNAs was evaluated in maternal plasma samples from patients with EA and JIA. Our findings revealed significant under expression of the four tsRNAs in the maternal plasma of patients with EA, whereas no expression differences were observed in the maternal plasma of patients with JIA. These results implied the potential application for the prenatal diagnosis and early intervention of many kinds of gastrointestinal atresia.

During the biomarker screening period, tRF-58:76-Tyr-GTA-2-M3 demonstrated the highest diagnostic accuracy. Our investigation focused on tRF-58:76-Tyr-GTA-2-M3 to ascertain its potential role in DA development. Accordingly, we investigated the expression of tRF-58:76-Tyr-GTA-2-M3 and apoptosis-related proteins in four paired duodenal specimens from DA and normal fetuses. The results demonstrated that tRF-58:76-Tyr-GTA-2-M3 expression was associated with enhanced apoptosis in the duodenal tissues of DA fetuses compared to the normal group. To date, the biological function of tRF-58:76-Tyr-GTA-2-M3 remains unknown. The present

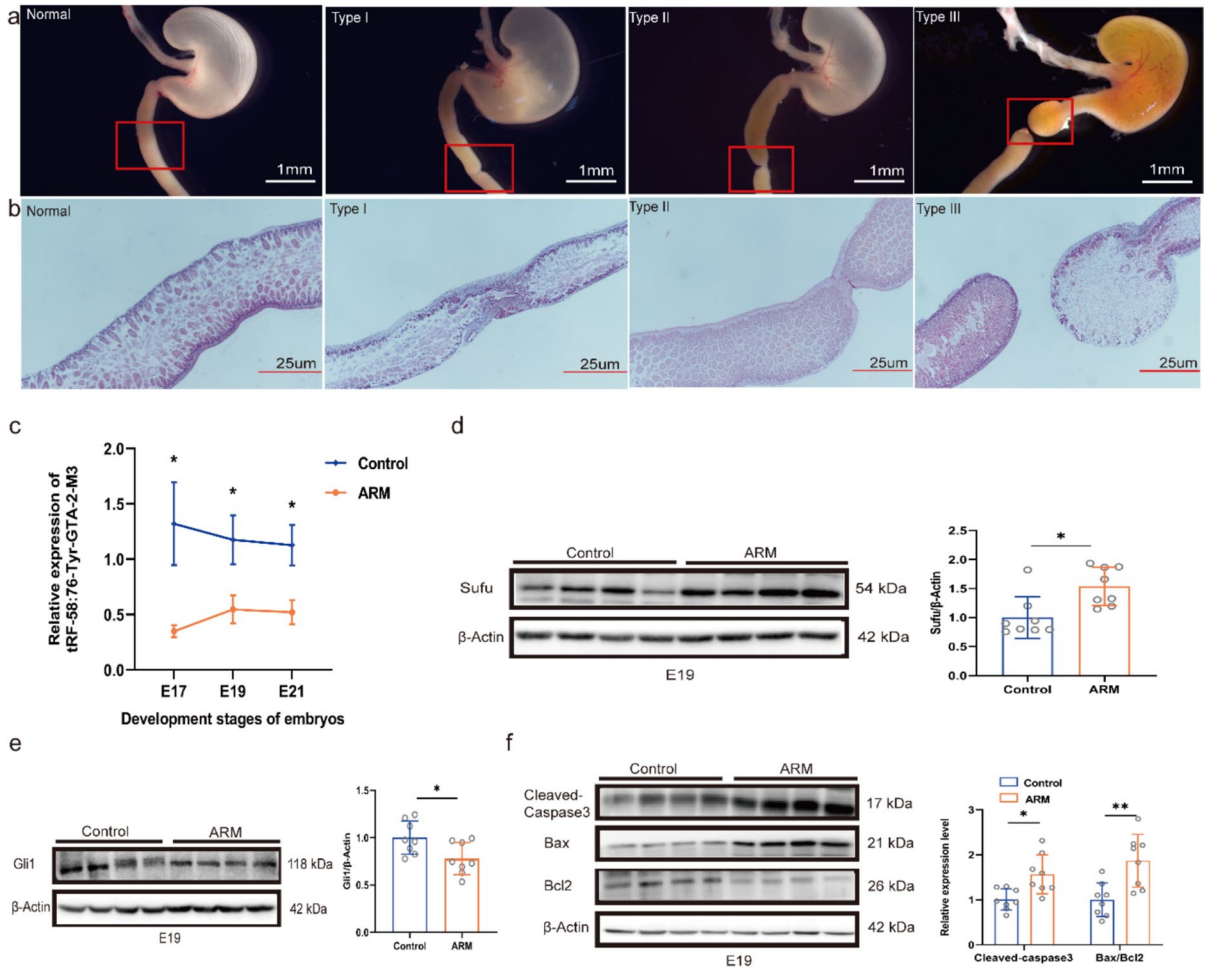

Fig. 7 Identification of DA in ARM and expression levels of tRF-58:76-Tyr-GTA-2-M3, Sufu, Gli1, and apoptosis-related proteins in the duodenum of ARM. **a**. Morphology of duodenum of normal and DA embryos at E21. **b**. HE staining images of the duodenum of normal and DA embryos at E21. **c**. qRT-PCR and change trend of tRF-58:76-Tyr-GTA-2-M3 in the duodenum of control and adriamycin-induced DA embryos at E17, E19, and E21. β-Actin as an endogenous control. Data are presented as the mean ± SD (n = 10, * $P < 0.05$; Unpaired t-test). **d**. Western Blot of the expression of Sufu protein in fetal duodenum of control and Adriamycin-induced DA embryos at E19. β-Actin as an endogenous control. Data are presented as the mean ± SD (n = 8, *$P < 0.05$; Unpaired t-test). **e**. Western Blot of the expression of Gli1 protein in fetal duodenum of control and Adriamycin-induced DA embryos at E19. β-Actin as an endogenous control. Data are presented as the mean ± SD (n = 8, * $P < 0.05$; Unpaired t-test). **f**. Western Blot of the expression of Cleaved-Caspase-3, Bax and Bcl2 in fetal duodenum of control and Adriamycin-induced rats at E19. β-Actin as an endogenous control. Data are presented as the mean ± SD (n = 8, * $P < 0.05$, ** $P < 0.01$; Unpaired t-test)

study demonstrated that tRF-58:76-Tyr-GTA-2-M3 overexpression in NCM460 cells resulted in a notable decrease in apoptosis. Given its markedly reduced levels in the duodenal tissues of DA fetuses, the apoptosis related to tRF-58:76-Tyr-GTA-2-M3 may play a pivotal role in DAs. Meanwhile, our study identified SUFU as a novel direct target gene of tRF-58:76-Tyr-GTA-2-M3, as supported by bioinformatics analysis and the verification that modulation of tRF-58:76-Tyr-GTA-2-M3 significantly alters SUFU levels. SUFU functions as a negative regulator of the Hedgehog/GLI1 signaling pathway and interacts with GLI1 to inhibit its nuclear translocation. GLI1 is a crucial transcription factor in the hedgehog pathway, which plays a pivotal role in mammalian gastrointestinal development and homeostasis. Its dysregulation may

contribute to the development of gastrointestinal malformations in humans (He et al. 2020; Zhang et al. 2017). Nevertheless, there is no evidence that SUFU and GLI1 are present in DAs. In this study, significant upregulation of SUFU and downregulation of GLI1 were observed in the duodenal tissues of DA fetuses. In vitro experiments in NCM460 cells indicated that SUFU silencing induced apoptosis, as demonstrated by remarkable alteration in the expression of apoptosis-related proteins. tRF-58:76-Tyr-GTA-2-M3 was predicted to target the 3′-UTR of *SUFU*, which was subsequently validated using a luciferase reporter assay. These findings suggested that tRF-58:76-Tyr-GTA-2-M3 may cause DA by inhibiting SUFU expression. Overexpression of tRF-58:76-Tyr-GTA-2-M3 enhanced GLI1 expression, whereas its inhibition resulted in decreased GLI1 levels. Furthermore, SUFU silencing promoted GLI1 expression. These findings collectively substantiate the assertion that tRF-58:76-Tyr-GTA-2-M3 exerts a regulatory influence on GLI1 expression and apoptosis by modulating the downstream target gene SUFU, underscoring its potential involvement in DA pathogenesis.

Advancements in prenatal genetic and obstetric ultrasound examination have enabled in intrauterine treatment of congenital diseases (Palanki et al. 2021). A previous study demonstrated that microinjection of miR-133a agomir into zebrafish embryos can counteract the production of reactive oxygen species and excessive proliferation of zebrafish central cells induced by trichloroethylene, significantly alleviating heart defects (Liu et al. 2022). Furthermore, the tRF-Gly inhibitor has been demonstrated to diminish liver steatosis in murine models of alcoholic fatty liver disease by upregulating the expression of Sirt1, consequently influencing downstream fatty acid production and β-oxidation pathways. This treatment may be a potential therapeutic target for alcoholic fatty liver disease (Zhong et al. 2019). Nevertheless, the potential therapeutic role of tsRNAs in fetal malformations remains unclear. Intraperitoneal administration of this treatment has demonstrated significant efficacy in the treatment of intestinal diseases (Wang et al. 2016). Liu et al. provided new insights into the prevention and treatment of colitis using intraperitoneal stem cell transplantation, which effectively controlled the progression and recurrence of the condition (Liu et al. 2022). Our team has conducted several studies demonstrating that injection of mesenchymal stem cells, adenoviral constructs containing specific genes, or miRNA mimics into the amniotic fluid during early fetal development can facilitate beneficial functional recovery from neural tube defects and anorectal malformations. These findings highlight the potential of prenatal therapeutic interventions to treat congenital malformations in embryos/fetuses (Liu et al. 2024, 2020; Ma et al. 2022a, 2020, 2022b; Wei et al. 2020). In this study, we observed a reduction in the expression of 58:76-Tyr-GTA-2-M3 in the duodenum of DA fetal rats at E17, E19, and E21. tRF-58:76-Tyr-GTA-2-M3 agomir was delivered to the uterus via intraperitoneal microinjection to relieve the inhibition of gene expression in Hedgehog pathway and inordinate apoptosis in the duodenum of fetal rats with DAs. The present findings demonstrate that intraperitoneal therapy in the duodenum facilitates the advancement of prenatally targeted therapy of DAs. However, ethical and practical considerations associated with prenatal intraperitoneal microinjection in human must be acknowledged. As with any fetal intervention, both the mother and the fetus are involved, potential complications such as infection, preterm labor, and fetal loss must be carefully considered. These concerns underscore the need for extensive preclinical validation and rigorous safety assessment before any clinical translation can be contemplated.

There are several limitations in our study. First, this pilot study with a small human sample and single-center design lacking validation of earlier DA cases and patient diversity, may limit the reliability and generalizability of the findings; thus, multicenter studies with larger and more diverse cohorts are warranted for confirmation. Second, the adriamycin rat model, while valuable, is constrained by off-target toxicity, litter-to-litter variability in DA penetrance, and species-specific foregut development differences. Future studies require using cross-validation in complementary models such as genetic mouse mutants and human foregut organoids. Finally, the involvement of additional target genes regulated by tRF-58:76-Tyr-GTA-2-M3 cannot be ruled out. Therefore, more studies are warranted to comprehensively elucidate the multifaceted roles of tRF-58:76-Tyr-GTA-2-M3 beyond its effects on apoptosis.

In summary, this study identified four pregnancy-related tsRNAs, including tRF-61:78-chrM. Leu-TAA, tRF-60:77-Ile-AAT-1-M4, tRF-57:76-Arg-ACG-1-M2, and tRF-58:76-Tyr-GTA-2-M3 have been identified as

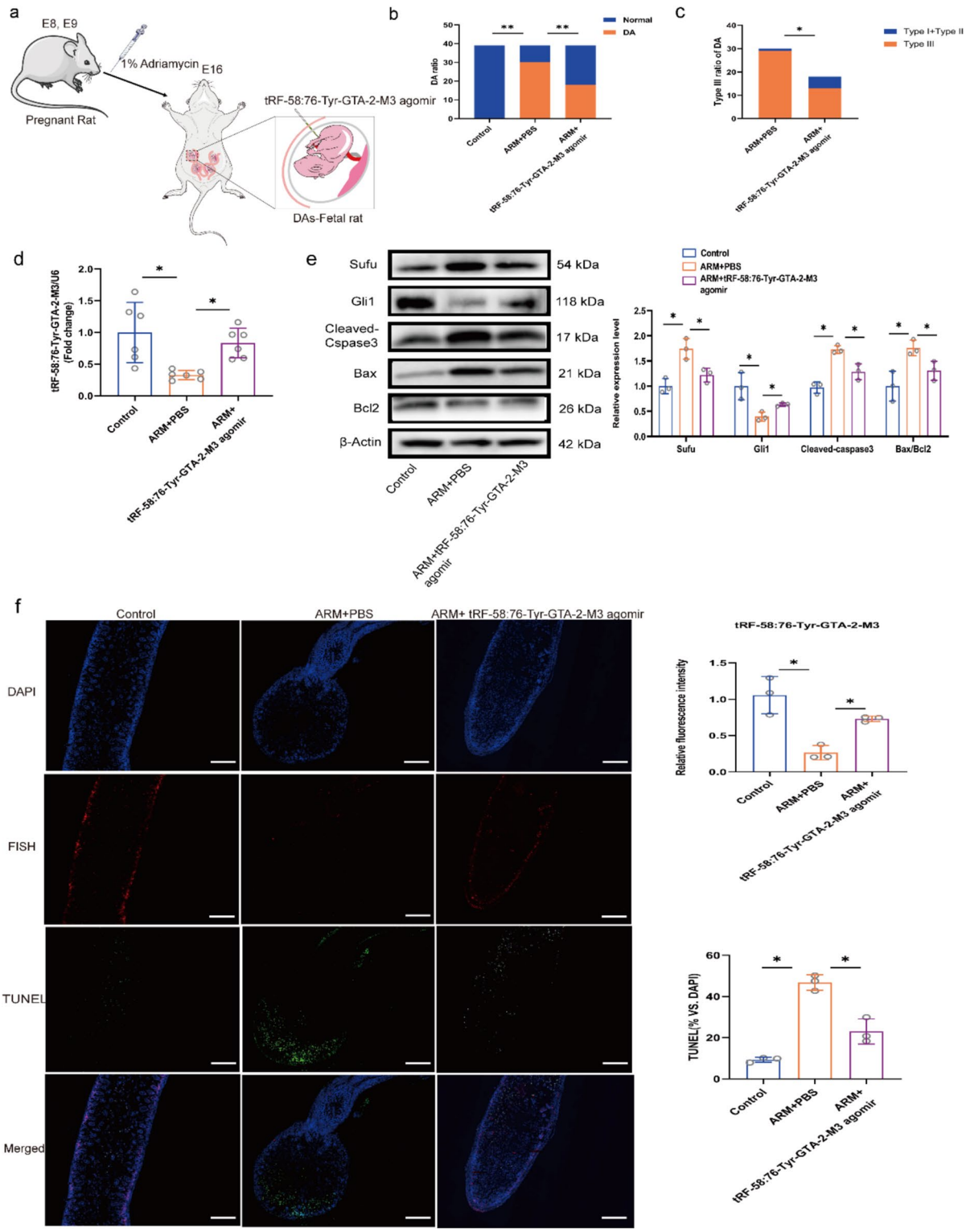
a
E8, E9
1% Adriamycin
E16
Pregnant Rat
tRF-58:76-Tyr-GTA-2-M3 agomir
DAs-Fetal rat
b
Normal
DA
DA ratio
Control
ARM+PBS
ARM+ tRF-58:76-Tyr-GTA-2-M3 agomir
c
Type I+Type II
Type III
Type III ratio of DA
d
tRF-58:76-Tyr-GTA-2-M3/U6 (Fold change)
e
Sufu
Gli1
Cleaved-Cspase3
Bax
Bcl2
β-Actin
54 kDa
118 kDa
17 kDa
21 kDa
26 kDa
42 kDa
Control
ARM+PBS
ARM+tRF-58:76-Tyr-GTA-2-M3 agomir
Relative expression level
Sufu
Gli1
Cleaved-caspase3
Bax/Bcl2
f
Control
ARM+PBS
ARM+ tRF-58:76-Tyr-GTA-2-M3 agomir
DAPI
FISH
TUNEL
Merged
tRF-58:76-Tyr-GTA-2-M3
Relative fluorescence intensity
TUNEL(% VS. DAPI)

◂**Fig. 8** Intraperitoneal microinjection of tRF-58:76-Tyr-GTA-2-M3 agomir exhibited therapeutic effect by reducing apoptosis **a**. Schematic representation of the intraperitoneal microinjection procedure for delivering tRF-58:76-Tyr-GTA-2-M3 agomir into E16 embryos. The capillary injection needle (green) traversed the uterine wall (pink) and the amnion (gray) before reaching the abdominal cavity. **b**. The number of embryos of DA in the control, ARM + PBS, and ARM + tRF-58:76-Tyr-GTA-2-M3 agomir groups (**$P < 0.01$; Chi-square test). **c**. The number of embryos of type III DA in the control, ARM + PBS, and ARM + tRF-58:76-Tyr-GTA-2-M3 agomir groups (*$P < 0.05$; Chi-square test). **d**. qRT-PCR was used to detect the expression of tRF-58:76-Tyr-GTA-2-M3 in the duodenum of fetal rat in each group. β-Actin as an endogenous control. Data are presented as the mean ± SD (n = 6, * $P < 0.05$; one-way ANOVA with Turkey correction). **e**. Western Blot were used to detect the expression of Sufu, Gli1, Cleaved-Caspase 3, Bax and Bcl-2 in the duodenum of fetal rat in each group. β-Actin as an endogenous control. Data are presented as the mean ± SD (n = 3, * $P < 0.05$; one-way ANOVA with Turkey correction). **f**. Representative images of FISH and TUNEL double staining showing the fluorescence of tRF-58:76-Tyr-GTA-2-M3 (red) and the TUNEL signal (green) in the E21 duodenum. Nuclei were counterstained with DAPI (blue). Statistical analysis of the fluorescence intensity and percentage of TUNEL-positive signals colocalized with strong tRF-58:76-Tyr-GTA-2-M3 expression. Data are presented as the mean ± SD. Scale bar = 20 μm (n = 3, * $P < 0.05$, one-way ANOVA with Turkey correction)

novel and promising fetal DA biomarkers. tRF-58:76-Tyr-GTA-2-M3 has been identified as a key factor in DA pathogenesis. The tRF-58:76-Tyr-GTA-2-M3/SUFU/Hedgehog-GLI1 regulatory axis plays a crucial role in DA pathogenesis by modulating apoptosis. Moreover, intraperitoneal microinjection of tRF-58:76-Tyr-GTA-2-M3 agomir into fetal rats resulted in the decreased expression of apoptosis-related genes, which was achieved by inhibiting SUFU and increasing GLI1 expression. This suggests tRF-58:76-Tyr-GTA-2-M3 as a potential therapeutic target for DA. The potential application of the identified tsRNA biomarkers as non-invasive tools for the risk assessment of DA, which in conjunction with imaging findings, particularly ultrasound, could support timely clinical decision-making and individualized prenatal care. Taken together, our findings highlight the potential utility of circulating plasma tsRNAs not only as predictive biomarkers, but also therapeutic targets for DA.

Acknowledgements We thank all individuals who take part in this research. The graphic abstract was drawed by Figdraw (www.figdraw.com).

Author contributions Xinyue Meng, Wei Sun and Zhengwei Yuan designed the experiments. Xinyue Meng, Wei Sun, and Jia Xue collected blood sample and prepared plasma. Xinyue Meng, Wenting Luo, Xiaowei Wei and Yiwen He collected data and performed experiments for the study. Xinyue Meng and Wenting Luo analyzed the data. Xinyue Meng and Zhengwei Yuan wrote the first draft of the paper. Xinyue Meng, Xiaowei Wei, Wei Ma, Dan Liu, Shanshan Jia, Hui Gu, Songying Cao, Dongxue Ding, Yiwen He, Wanqi Huang, Jia Xue, Wenting Luo, Wei Sun, Zhengwei Yuan contributed to the writing of the paper. All authors read and approved the final manuscript.

Funding The research was supported by the National Natural Science Foundation of China (NO. 82171649, 82402313), National Key Research and Development Program (No.2021YFC2701003), LiaoNing Revitalization Talents Program (No. XLYC1902099), The Science and Technology Plan Joint Plan Project of Liaoning Province (2024-BSLH-317), the Science and Technology Plan Project of Liaoning Province (2023 JH2/20200082) and Applied basic research program for young scholars of Liaoning Province (2023 JH2/101600026).

Data availability No datasets were generated or analysed during the current study.

Declarations

Ethnic approval All human participants provided written informed consent, and the study was conducted in accordance with the principles of the Declaration of Helsinki, receiving approval from the Ethics Committee of Shengjing Hospital of China Medical University (Approval No. 2017PS264 K). All procedures involving animal use adhered to the National Institutes of Health Guide for the Care and the Animal Ethics Committee of Shengjing Hospital of China Medical University (Approval No. 2020PS153 K).

Conflict of interests The authors declare no competing interests.

References

Aboughalia H, Bastawrous S, Revzin MV, Delaney SS, Katz DS, Moshiri M. Imaging findings in association with altered maternal alpha-fetoprotein levels during pregnancy. Abdom Radiol (New York). 2020;45:3239–57. https://doi.org/10.1007/s00261-020-02499-2.

An D, Wei X, Li H, Gu H, Huang T, Zhao G, Liu B, Wang W, Chen L, Ma W, Zhang H, Cao S, Yuan Z. Identification of PCSK9 as a novel serum biomarker for the prenatal diagnosis of neural tube defects using iTRAQ quantitative proteomics. Sci Rep. 2015;5:17559. https://doi.org/10.1038/srep17559.

Basu R, Burge DM. The effect of antenatal diagnosis on the management of small bowel atresia. Pediatr Surg Int. 2004;20:177–9. https://doi.org/10.1007/s00383-004-1140-8.

Best KE, Tennant PW, Addor MC, Bianchi F, Boyd P, Calzolari E, Dias CM, Doray B, Draper E, Garne E, Gatt M, Greenlees R, Haeusler M, Khoshnood B, McDonnell B, Mullaney C, Nelen V, Randrianaivo H, Rissmann A, Salvador J, Tucker D, Wellesly D, Rankin J. Epidemiology of small intestinal atresia in Europe: a register-based study. Arch Dis Child Fetal Neonatal Ed. 2012;97:F353–8. https://doi.org/10.1136/fetalneonatal-2011-300631.

Bethell GS, Long AM, Knight M, Hall NJ, Baps C. Congenital duodenal obstruction in the UK: a population-based study. Arch Dis Child Fetal Neonatal Ed. 2020;105:178–83. https://doi.org/10.1136/archdischild-2019-317085.

Bittencourt DG, Barini R, Marba S, Sbragia L. Congenital duodenal obstruction: does prenatal diagnosis improve the outcome? Pediatr Surg Int. 2004;20:582–5. https://doi.org/10.1007/s00383-004-1235-2.

Botham RA, Franco M, Reeder AL, Lopukhin A, Shiota K, Yamada S, Nichol PF. Formation of duodenal atresias in fibroblast growth factor receptor 2IIIb-/- mouse embryos occurs in the absence of an endodermal plug. J Pediatr Surg. 2012;47:1369–79. https://doi.org/10.1016/j.jpedsurg.2012.02.001.

Chen L, Gu H, Li J, Yang ZY, Sun X, Zhang L, Shan L, Wu L, Wei X, Zhao Y, Ma W, Zhang H, Cao S, Huang T, Miao J, Yuan Z. Comprehensive maternal serum proteomics identifies the cytoskeletal proteins as non-invasive biomarkers in prenatal diagnosis of congenital heart defects. Sci Rep. 2016;6:19248. https://doi.org/10.1038/srep19248.

Chen X, Zheng Y, Lei A, Zhang H, Niu H, Li X, Zhang P, Liao M, Lv Y, Zhu Z, Pan C, Dong W, Chen H, Wu D, Liu W, Hamer G, Zeng S, Zeng W. Early cleavage of preimplantation embryos is regulated by tRNA(Gln-TTG)-derived small RNAs present in mature spermatozoa. J Biol Chem. 2020;295:10885–900. https://doi.org/10.1074/jbc.RA120.013003.

Chen X, Sun Q, Zheng Y, Liu Z, Meng X, Zeng W, Lu H. Human sperm tsRNA as potential biomarker and therapy target for male fertility. Reproduction. 2021;161:111–22. https://doi.org/10.1530/rep-20-0415.

Cheng W, Tam PK. Apoptosis in murine duodenum during embryonic development. Pediatr Surg Int. 2000;16:485–7. https://doi.org/10.1007/s003830000408.

Cole C, Sobala A, Lu C, Thatcher SR, Bowman A, Brown JW, Green PJ, Barton GJ, Hutvagner G. Filtering of deep sequencing data reveals the existence of abundant Dicer-dependent small RNAs derived from tRNAs. RNA. 2009;15:2147–60. https://doi.org/10.1261/rna.1738409.

Dong N, Gu H, Liu D, Wei X, Ma W, Ma L, Liu Y, Wang Y, Jia S, Huang J, Wang C, He X, Huang T, He Y, Zhang Q, An D, Bai Y, Yuan Z. Complement factors and alpha-fetoprotein as biomarkers for noninvasive prenatal diagnosis of neural tube defects. Ann N Y Acad Sci. 2020;1478:75–91. https://doi.org/10.1111/nyas.14443.

Fairbanks TJ, Kanard R, Del Moral PM, Sala FG, De Langhe S, Warburton D, Anderson KD, Bellusci S, Burns RC. Fibroblast growth factor receptor 2 IIIb invalidation–a potential cause of familial duodenal atresia. J Pediatr Surg. 2004;39:872–4. https://doi.org/10.1016/j.jpedsurg.2004.02.026.

Fairbanks TJ, Sala FG, Kanard R, Curtis JL, Del Moral PM, De Langhe S, Warburton D, Anderson KD, Bellusci S, Burns RC. The fibroblast growth factor pathway serves a regulatory role in proliferation and apoptosis in the pathogenesis of intestinal atresia. J Pediatr Surg. 2006;41:132–6. https://doi.org/10.1016/j.jpedsurg.2005.10.054. (discussion -6).

França WM, Gonçalves A, Moraes SG, Pereira LA, Sbragia L. Esophageal atresia and other visceral anomalies in a modified Adriamycin rat model and their correlations with amniotic fluid volume variations. Pediatr Surg Int. 2004;20:602–8. https://doi.org/10.1007/s00383-004-1240-5.

Gu H, Li H, Zhang L, Luan H, Huang T, Wang L, Fan Y, Zhang Y, Liu X, Wang W, Yuan Z. Diagnostic role of microRNA expression profile in the serum of pregnant women with fetuses with neural tube defects. J Neurochem. 2012;122:641–9. https://doi.org/10.1111/j.1471-4159.2012.07812.x.

Gu H, Chen L, Xue J, Huang T, Wei X, Liu D, Ma W, Cao S, Yuan Z. Expression profile of maternal circulating microRNAs as non-invasive biomarkers for prenatal diagnosis of congenital heart defects. Biomed Pharmacother. 2019;109:823–30. https://doi.org/10.1016/j.biopha.2018.10.110.

Haeusler MC, Berghold A, Stoll C, Barisic I, Clementi M. Prenatal ultrasonographic detection of gastrointestinal obstruction: results from 18 European congenital anomaly registries. Prenat Diagn. 2002;22:616–23. https://doi.org/10.1002/pd.341.

He S, Yang F, Yang M, An W, Maguire EM, Chen Q, Xiao R, Wu W, Zhang L, Wang W, Xiao Q. miR-214-3p-Sufu-GLI1 is a novel regulatory axis controlling inflammatory smooth muscle cell differentiation from stem cells and neointimal hyperplasia. Stem Cell Res Ther. 2020;11:465. https://doi.org/10.1186/s13287-020-01989-w.

Hemming V, Rankin J. Small intestinal atresia in a defined population: occurrence, prenatal diagnosis and survival. Prenat Diagn. 2007;27:1205–11. https://doi.org/10.1002/pd.1886.

Huang W, Huang T, Liu Y, Fu J, Wei X, Liu D, Ma W, Gu H, Yuan Z. Nuclear factor I-C disrupts cellular homeostasis between autophagy and apoptosis via miR-200b-Ambra1 in neural tube defects. Cell Death Dis. 2021;13:17. https://doi.org/10.1038/s41419-021-04473-2.

Jia S, Zhang Q, Wang Y, Wang Y, Liu D, He Y, Wei X, Gu H, Ma W, Luo W, Yuan Z. PIWI-interacting RNA sequencing profiles in maternal plasma-derived exosomes reveal novel non-invasive prenatal biomarkers for the early diagnosis of nonsyndromic cleft lip and palate. EBioMedicine. 2021;65:103253. https://doi.org/10.1016/j.ebiom.2021.103253.

Jones MLM, Sarila G, Chapuis P, Hutson JM, King SK, Teague WJ. The role of fibroblast growth factor 10 signaling in Duodenal Atresia. Front Pharmacol. 2020;11:250. https://doi.org/10.3389/fphar.2020.00250.

Lee YS, Shibata Y, Malhotra A, Dutta A. A novel class of small RNAs: tRNA-derived RNA fragments (tRFs). Genes Dev. 2009;23:2639–49. https://doi.org/10.1101/gad.1837609.

Liu YS, Gu H, Huang TC, Wei XW, Ma W, Liu D, He YW, Luo WT, Huang JT, Zhao D, Jia SS, Wang F, Zhang T, Bai YZ, Wang WL, Yuan ZW. miR-322 treatment rescues cell apoptosis and neural tube defect formation through silencing NADPH oxidase 4. CNS Neurosci Ther. 2020;26:902–12. https://doi.org/10.1111/cns.13383.

Liu J, Lai X, Bao Y, Xie W, Li Z, Chen J, Li G, Wang T, Huang W, Ma Y, Shi J, Zhao E, Xiang AP, Liu Q, Chen X. Intraperitoneally delivered mesenchymal stem cells alleviate experimental colitis through THBS1-mediated induction of IL-10-competent regulatory B cells. Front Immunol. 2022;13:853894. https://doi.org/10.3389/fimmu.2022.853894.

Liu P, Li Y, Yao Y, Wang W, Jia H, Bai Y, Yuan Z, Yang Z. Intra-amniotic delivery of tropomodulin 3 rescues cell apoptosis induced by miR-200b-3p upregulation via non-canonical nuclear factor kappa B pathways in ethylene thiourea induced anorectal malformations fetal rat. Ecotoxicol Environ Saf. 2024;284:116918. https://doi.org/10.1016/j.ecoenv.2024.116918.

Lu E, Wu L, Chen B, Xu S, Fu Z, Wu Y, Wu Y, Gu H. Maternal Serum tRNA-Derived Fragments (tRFs) as potential candidates for diagnosis of fetal congenital heart disease. J Cardiovasc Dev Dis. 2023;10. https://doi.org/10.3390/jcdd10020078.

Ma W, Wei X, Gu H, Liu D, Luo W, An D, Bai Y, Yuan Z. Therapeutic potential of adenovirus-encoding brain-derived neurotrophic factor for spina bifida aperta by intra-amniotic delivery in a rat model. Gene Ther. 2020;27:567–78. https://doi.org/10.1038/s41434-020-0131-2.

Ma L, Wei X, Ma W, Liu Y, Wang Y, He Y, Jia S, Wang Y, Luo W, Liu D, Huang T, Yan J, Gu H, Bai Y, Yuan Z. Neural stem cell-derived exosomal netrin1 contributes to neuron differentiation of mesenchymal stem cells in therapy of spinal bifida aperta. Stem Cells Transl Med. 2022a;11:539–51. https://doi.org/10.1093/stcltm/szac009.

Ma W, Wei X, Gu H, Liu D, Luo W, Cao S, Jia S, He Y, Chen L, Bai Y, Yuan Z. Intra-amniotic transplantation of brain-derived neurotrophic factor-modified mesenchymal stem cells treatment for rat fetuses with spina bifida aperta. Stem Cell Res Ther. 2022b;13:413. https://doi.org/10.1186/s13287-022-03105-6.

Merrot T, Anastasescu R, Pankevych T, Tercier S, Garcia S, Alessandrini P, Guys JM. Duodenal duplications. Clinical characteristics, embryological hypotheses, histological findings, treatment. Eur J Pediatr Surg. 2006;16:18–23. https://doi.org/10.1055/s-2006-923798.

Palanki R, Peranteau WH, Mitchell MJ. Delivery technologies for in utero gene therapy. Adv Drug Deliv Rev. 2021;169:51–62. https://doi.org/10.1016/j.addr.2020.11.002.

Patterson KN, Cruz S, Nwomeh BC, Diefenbach KA. Congenital duodenal obstruction - Advances in diagnosis, surgical management, and associated controversies. Semin Pediatr Surg. 2022;31:151140. https://doi.org/10.1016/j.sempedsurg.2022.151140.

Qi B, Diez-Pardo JA, Navarro C, Tovar JA. Narrowing the embryologic window of the adriamycin-induced fetal rat model of esophageal atresia and tracheoesophageal fistula. Pediatr Surg Int. 1996;11:444–7. https://doi.org/10.1007/bf00180079.

Ramalho-Santos M, Melton DA, McMahon AP. Hedgehog signals regulate multiple aspects of gastrointestinal development. Development. 2000;127:2763–72. https://doi.org/10.1242/dev.127.12.2763.

Romero R, Ghidini A, Costigan K, Touloukian R, Hobbins JC. Prenatal diagnosis of duodenal atresia: does it make any difference? Obstet Gynecol. 1988;71:739–41.

Shi J, Zhang Y, Tan D, Zhang X, Yan M, Zhang Y, Franklin R, Shahbazi M, Mackinlay K, Liu S, Kuhle B, James ER, Zhang L, Qu Y, Zhai Q, Zhao W, Zhao L, Zhou C, Gu W, Murn J, Guo J, Carrell DT, Wang Y, Chen X, Cairns BR, Yang XL, Schimmel P, Zernicka-Goetz M, Cheloufi S, Zhang Y, Zhou T, Chen Q. PANDORA-seq expands the repertoire of regulatory small RNAs by overcoming RNA modifications. Nat Cell Biol. 2021;23:424–36. https://doi.org/10.1038/s41556-021-00652-7.

Tian H, Hu Z, Wang C. The Therapeutic Potential of tRNA-derived Small RNAs in Neurodegenerative Disorders. Aging Dis. 2022;13:389–401. https://doi.org/10.14336/ad.2021.0903.

van den Brink GR. Hedgehog signaling in development and homeostasis of the gastrointestinal tract. Physiol Rev. 2007;87:1343–75. https://doi.org/10.1152/physrev.00054.2006.

Wang M, Liang C, Hu H, Zhou L, Xu B, Wang X, Han Y, Nie Y, Jia S, Liang J, Wu K. Intraperitoneal injection (IP), Intravenous injection (IV) or anal injection (AI)? Best way for mesenchymal stem cells transplantation for colitis. Sci Rep. 2016;6:30696. https://doi.org/10.1038/srep30696.

Wang Y, Ma L, Jia S, Liu D, Gu H, Wei X, Ma W, Luo W, Bai Y, Wang W, Yuan Z. Serum exosomal coronin 1A and dynamin 2 as neural tube defect biomarkers. J Mol Med (Berl). 2022;100:1307–19. https://doi.org/10.1007/s00109-022-02236-w.

Wei X, Ma W, Gu H, Liu D, Luo W, Bai Y, Wang W, Lui VCH, Yang P, Yuan Z. Transamniotic mesenchymal stem cell therapy for neural tube defects preserves neural function

through lesion-specific engraftment and regeneration. Cell Death Dis. 2020;11:523. https://doi.org/10.1038/s41419-020-2734-3.

Weng Q, Wang Y, Xie Y, Yu X, Zhang S, Ge J, Li Z, Ye G, Guo J. Extracellular vesicles-associated tRNA-derived fragments (tRFs): biogenesis, biological functions, and their role as potential biomarkers in human diseases. J Mol Med (Berl). 2022;100:679–95. https://doi.org/10.1007/s00109-022-02189-0.

Zhang Z, Shen L, Law K, Zhang Z, Liu X, Hua H, Li S, Huang H, Yue S, Hui CC, Cheng SY. Suppressor of fused chaperones gli proteins to generate transcriptional responses to sonic hedgehog signaling. Mol Cell Biol. 2017;37. https://doi.org/10.1128/mcb.00421-16.

Zhong F, Hu Z, Jiang K, Lei B, Wu Z, Yuan G, Luo H, Dong C, Tang B, Zheng C, Yang S, Zeng Y, Guo Z, Yu S, Su H, Zhang G, Qiu X, Tomlinson S, He S. Complement C3 activation regulates the production of tRNA-derived fragments Gly-tRFs and promotes alcohol-induced liver injury and steatosis. Cell Res. 2019;29:548–61. https://doi.org/10.1038/s41422-019-0175-2.